Czech Technical University in Prague

Faculty of Electrical Engineering

BACHELOR THESIS

Jiří Minarik

Yaw Stabilization of 4 Wheel Steering Cars

Department of Control Engineering

Supervisor of the bachelor thesis: Ing. Denis Efremov

Study programme: Cybernetics and Robotics

Prague 2019

BACHELOR'S THESIS ASSIGNMENT

I. Personal and study details

Student's name: **Minarik Jiří** Personal ID number: **466174**

Faculty / Institute: **Faculty of Electrical Engineering**

Department / Institute: **Department of Control Engineering**

Study program: **Cybernetics and Robotics**

II. Bachelor's thesis details

Bachelor's thesis title in English:

Yaw Stabilization of 4 Wheel Steering Cars

Bachelor's thesis title in Czech:

Stabilizace stáčivé rychlosti pro vozidlo se čtyřmi řídiltelnými koly

Guidelines:

The goal of the thesis is to investigate benefits and possible control limitations of 4 wheel steering (4WS) ground vehicles, discuss state-of-the-art solutions coming from industry and academia, implement the suitable approach, and test it on provided car simulator.
1. Adopt a single-track model.
2. Discuss the pros and cons of 4WS cars in comparison to conventional 2WS vehicles.
3. Review control solutions of yaw stabilization applied in the automotive industry (Audi, Porsche, Mazda, etc.) and yaw control algorithms published in the literature.
4. Implement suitable hierarchical control approaches from the literature
5. Suggest control methods improvements based on outcomes from point 3 and implement such augmentations
6. Provide validation and comparison of developed control systems.

Bibliography / sources:

[1] Ackermann, J. (1994). Robust decoupling, ideal steering dynamics and yaw stabilization of 4WS cars. Automatica, 30(11), 1761-1768.
[2] Schramm, D., Hiller, M., & Bardini, R. (2014). Vehicle dynamics. Modeling and Simulation. Berlin, Heidelberg, 151.
[3] Franklin, G. F., Powell, J. D., Emami-Naeini, A., & Powell, J. D. (1994). Feedback control of dynamic systems (Vol. 3). Reading, MA: Addison-Wesley.
[4] Tsurumiya, O., Izawa, M., Abe, M., & Nonaga, I. (1993). U.S. Patent No. 5,189,616. Washington, DC: U.S. Patent and Trademark Office.
[5] Sudale, S. (2016). U.S. Patent No. 9,409,597. Washington, DC: U.S. Patent and Trademark Office.
[6] Mori, K., & Irie, N. (1990). U.S. Patent No. 4,947,326. Washington, DC: U.S. Patent and Trademark Office.

Name and workplace of bachelor's thesis supervisor:

Ing. Denis Efremov, Department of Control Engineering, FEE

Name and workplace of second bachelor's thesis supervisor or consultant:

Date of bachelor's thesis assignment: **24.01.2019** Deadline for bachelor thesis submission: **24.05.2019**

Assignment valid until:
by the end of summer semester 2019/2020

Ing. Denis Efremov	prof. Ing. Michael Šebek, DrSc.	prof. Ing. Pavel Ripka, CSc.
Supervisor's signature	Head of department's signature	Dean's signature

III. Assignment receipt

The student acknowledges that the bachelor's thesis is an individual work. The student must produce his thesis without the assistance of others, with the exception of provided consultations. Within the bachelor's thesis, the author must state the names of consultants and include a list of references.

. _____
Date of assignment receipt

_____
Student's signature

Acknowledgements

I would like to thank my supervisor, Ing. Denis Efremov. I am incredibly thankful to him for sharing expertise, and valuable guidance extended to me, and Bc. Vít Cibulka for shared twin track model.

Also, I take this opportunity to express gratitude to all of the Department faculty of Electrical Engineering members for their help and support. I also thank my mom for the words of encouragement, support, and attention.

I as well place on record, my sense of gratitude to all, who directly or indirectly, have lent me their help.

I hereby declare that I have completed this thesis with the topic "Yaw Stabilization of 4 Wheel Steering Cars" independently and that I have included a full list of used references. I have no objection to the usage of this work in compliance with the act §60 Zákon č. 121/2000 Sb. (copyright law).

In ..... date ..... signature of the author

Abstrakt:

Tato bakalářská práce je zaměřena na změnu vstupního signálu řidiče z volantu pro získání žádoucích řídících úhlů na přední a zadní kola ke zlepšení manévrovatelnosti auta. Jsou zde diskutovány dvě implementované metody z automobilového průmyslu a vědy. Následně jsou obě otestovány na nedotáčivých a přetáčivých autech stejně jako na nově navržených řešeních, které jsou odvozeny na jedno stopém modelu během této práce. Veškeré testování jízdy je provedeno na dvou stopém modelu.

Klíčová slova: Regulátor, Pacejka Magic Formula, Jednostopý model, Dvoustopý model, Steer-by-wire, Přetáčivé a nedotáčivé auto, Sledování stáčivé rychlosti, Čtyřkolový řídící systém, Poloměr otáčení, Střed otáčení.

Abstract:

This bachelor thesis is focused on altering the driver's input from the steering wheel to get desired steering angles on both front and rear wheels to increase the vehicle's maneuverability. It is discussing two already implemented methods from the automotive industry and automotive science. Then, both are tested on understeering and oversteering car's setups as well as new proposed solutions that are derived on a single-track model during this work. All ride-tests are done on provided twin-track model.

Keywords: Controller, Pacejka Magic Formula, Single-track, Twin-track, Steer-by-wire, Oversteering and understeering car, Yaw rate tracking, Four-wheel steering system, Turning radius and center.

Contents

1. Introduction

Nowadays, many cars are made with Steer-by-wire technology, meaning that vehicle can be controlled only by electric or electric-mechanical systems instead of just conventional mechanical systems. As a result, it is possible to alter drivers steering wheel input completely and change it to one that is the best in a given situation and thus benefits both driver and car.

Furthermore, such technology can be used for the implementation of a four-wheel steering system. The immediate benefits are:

- Stability - The four-wheel steering system is more stable to changes of weather conditions or terrain where rear wheels are capable of compensating such instabilities.
- Smaller Turns – If rear wheels are pointed in the opposite direction than front wheels, vehicles turning radius is smaller and such capable of making the same turns with less effort and less considerable space requirements.
- Double Lane Change – Vehicles with four-wheel steering system are capable of "crab walk" between lanes when both steering angles are pointed in the same direction in front and rear wheels, thus making maneuver faster and smoother.
- Smoother Steering – Due to rear wheels helping in cornering maneuvers, cars have better and faster response to drivers input from the steering wheel.
- Redundancy - When front axle of the car is inresponsive due to failure, vehicle can be still controlled by wheels on rear axle.
- Better Terrain Performance – When front wheels are stuck, rear wheels are capable of forcing car out and helping it to climb steeper terrain.

On the other hand, disadvantages are almost none. Some are expressed in the higher vulnerability of a system because of complicated installments and increased manufacturing cost due to the increased number of components needed. The main problem is developing control algorithms, which must exist as a layer between driver's controllers (pedals and steering wheel) and real actuators (motors and servos). The idea of the considered system that is completely stable and safe, which is possible with the right controller, can help in the development of better self-driving cars and finally put down any dangers of car accidents.

Even though, some solutions of four-wheel steering cars already exist, there is still no final solution. That is why some of them are going to be discussed with new proposed concepts. See outline below.

1.1 Outline

The thesis is dived into eleven parts.

Firstly, the [**Introduction**] introduces the reader to the topic and outlines the whole work.

Secondly, the [**Objectives**] highlights assigments.

Next, [**State of the art**] and history of the four-wheel steering system will be discussed and already implemented solutions mentioned.

In the chapter [**Used modeling approaches**], the model of a car is derived, and it's difference to twin-track mentioned.

In the chapter [**Robust decouplind**] and [**Rear wheel steer angle control system**], already proposed concepts are evaluated and derived for the used model in [**Used modeling approaches**].

Additionally, the chapter [**Influence of Pacejka coefficients on behavior of a vehicle**] is discussing the dependency of Pacejka coefficients on oversteering and understeering tendency of a car.

Chapter [**Proposed solutions**] shows proposed control systems with controller and their derivation.

Simulation results are shown in [**Simlutation ride tests**], simulated on the twin-track model and compared to each other.

Fullfilled objectives are listed in [**Results**].

Results of tests and work are summarized in chapter [**Conclusion**].

2. Objectives

The objectives of this work are:

1. Adopt a single-track model.
2. Discuss the pros and cons of 4WS cars in comparison to conventional 2WS vehicles.
3. Review control solutions of yaw stabilization applied in the automotive industry (Audi, Porsche, Mazda, etc.) and yaw control algorithms published in the literature.
4. Implement suitable hierarchical control approaches from the literature.
5. Suggest control methods improvements based on outcomes from point 3 and implement such augmentations.
6. Provide validation and comparison of developed control systems.

3. State of the art

The beginnings of an ideology of four-wheel steering vehicle can be traced back to the year 1903 when first steam cars with the steered rear axle were produced. However, at that time, technology has not been able to support such systems yet. Then, the army took over and started implementing it during the First and the Second World Wars. The system was used for supply trucks improving their maneuverability and stability in difficult terrains and weather conditions. The renascence of 4WS came after the war in the 1960s where first road cars with that technology were manufactured. Many 4WS vehicles were sold in the U.S., Europe, and Australia because of their superior steering capabilities. Nevertheless, 4WS was almost entirely made of mechanical or semi-mechanical parts, which make a steering system very complicated and make cars even heavier and thus increasing their fuel consumption, leading to a decline in demand. However, with the arrival of new technologies, mainly Steer-by-wire technology, implementation of 4WS weights less and can be implemented into a conventional car without any difficulty.

There are already many companies like Audi, BMW, Nissan, and Toyota interested in such systems. Nowadays, the focus is on developing a 4WS car with a feedback control capable of steering a car along a predefined by driver's steering wheel path in such a way that the primary objective of the control law is focusing on tracking the driver's intended vehicle behavior and keep a car in the stable states of the system. Some solutions are already published. For instance, a predefined gain transformation between the rotation of rear wheels in the opposite or in the same direction as front wheels can be seen in [11]. Here, a desired rear wheel's steering angle is determined through state machine with a set of rules dependent on velocity and front wheels steering angle. Another implementation is logical switching mechanism between 2WS and 4WS discussed in [12], where the switching itself may be made by the driver or a controller with predefined values or based on outer parameters. Nissan company has made rear wheel steering in addition to the front without feedback where scaling is dependent only on velocity and front steering angle and is discussed in [**Rear wheel steer angle control system**]. In addition, the driving envelope, which defines stability state boundaries between maximum and minimum peaks of lateral forces dependent on tyre slip angles and thus providing one solution to the problem of spinning of the car, is depicted in [13]. The envelop itself is numerically calculated from tyre slip angles. In picture [3.1] is observed that driving envelop bounds are significantly increased with bigger rotational limits of δ_r angle.

In comparison to the industrial solutions, there were science teams which were trying to implement solutions based on the understanding of the vehicle dynamics and control theory. One of the group was headed by Jürgen Ackermann. One of their solutions will be discussed in chapter [**Robust decoupling**] and chapter [**Simlutation ride tests**]. More about Steer-by-wire and advantages and disadvantages of 4WS can be found in chapter [**Introduction**].

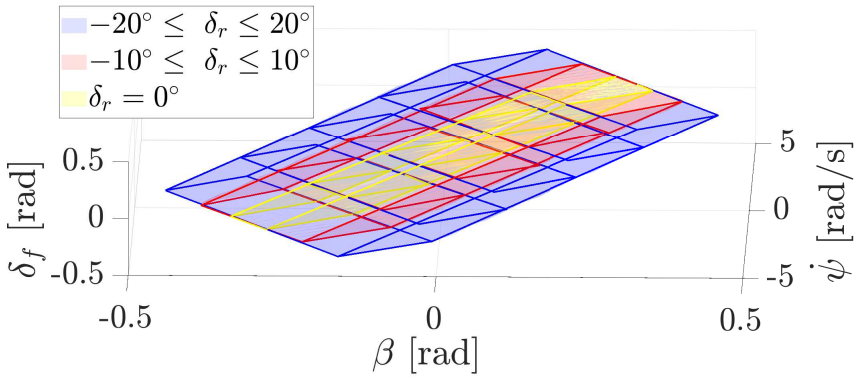

Figure 3.1: Comparison of the driving envelope for 2WS and 4WS vehicle from [13]

4. Used modeling approaches

4.1 Single-track

In this chapter, the model that is used throughout this work is derived, and it's linearized form is written down.

4.1.1 Forces and moments

First of all, the following assumptions are made:

- The forces and angles are the same on both front wheels and rear wheels of a vehicle.
- The position of a car can be described with one point named center of gravity (CG) which has no roll or pitch moment.
- The yaw moment direction is upwards (e.g., from the road to a car).
- The front wheels are lumped together into one which is in the center line of a car (e.g., the new wheel has the same distance between the left and right wheel and so is in the center). Same for rear wheels.
- The mass distribution is solid and that implies $m = m_f + m_r$ where m is mass of a car concentrated at CG, m_f and m_r are masses of front and rear axle respectively.

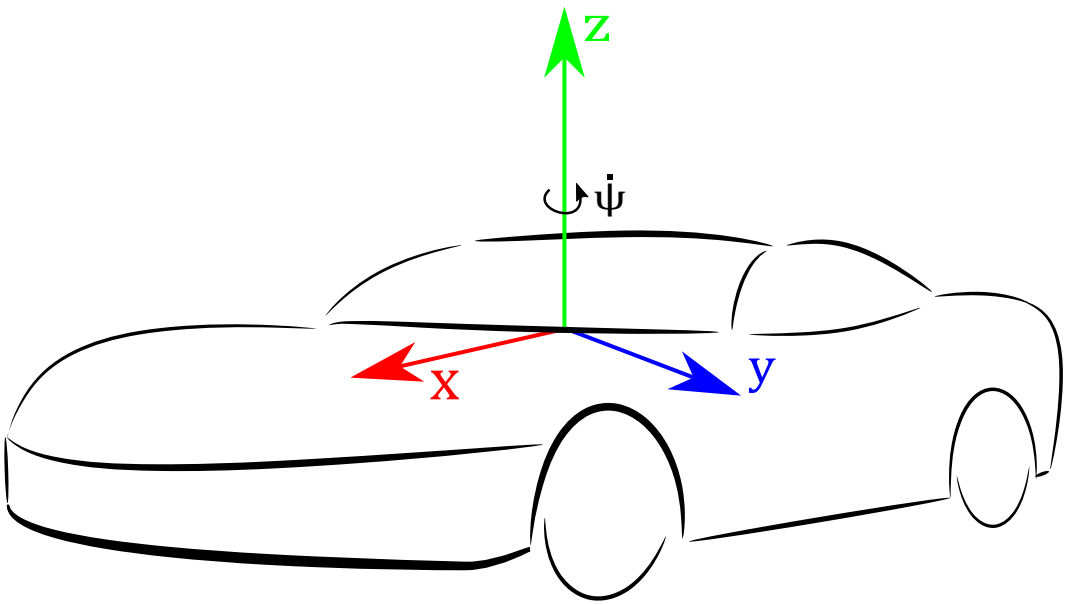

Figure 4.1: Vehicle coordinates system of a car with yaw motion $\dot{\psi}$

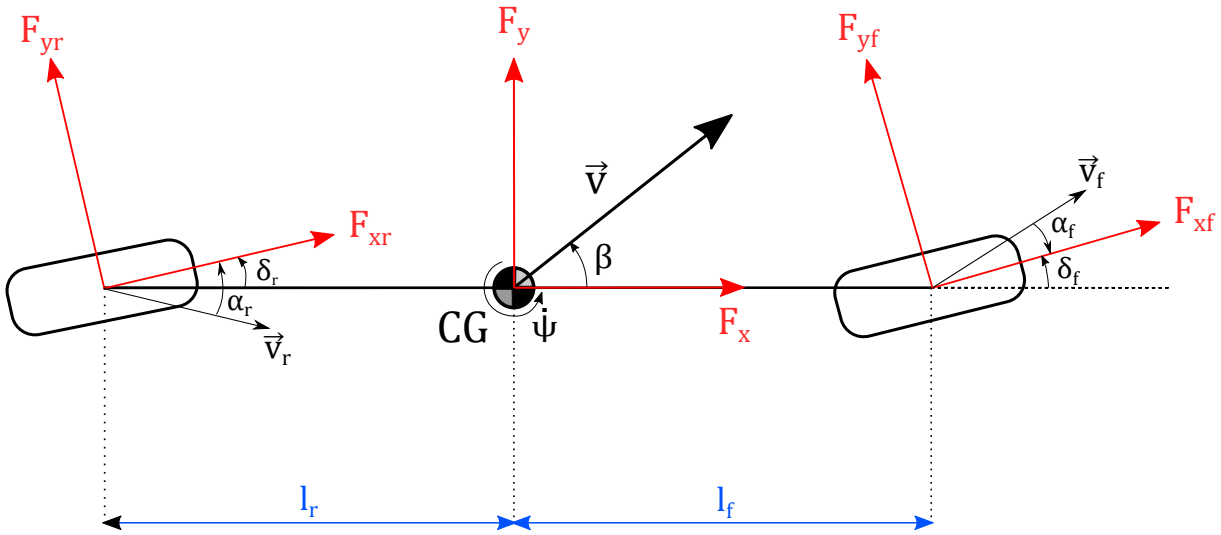

Figure 4.2: Single-track model of coordinates system in [4.1]

Now, the basic equations describing modeled system are derived. From picture [4.2] is clear that velocity

$$v^2 = v_x^2 + v_y^2 \,, \tag{4.1}$$

$$v_x = v \cdot \cos(\beta) \,, \tag{4.2}$$

$$v_y = v \cdot \sin(\beta) \,, \tag{4.3}$$

where v is velocity of car, β is the side slip angle and v_x and v_y are velocities in given axis. From the second fundamental law of motion by Sir Issac Newton also goes

$$F_x = a_x \cdot m \,, \tag{4.4}$$

$$F_y = a_y \cdot m \,, \tag{4.5}$$

where m is mass of vehicle, a_x and a_y are accelerations and F_x and F_y are forces in given axis. The formula $\dot{v} = a$ is valid. Once (4.4) and (4.5) are fit and with usage of (4.2) and (4.3) respectively the derivation derives following:

$$F_x = m \cdot \dot{v} \cdot \cos(\beta) - m \cdot v \cdot \sin(\beta) \cdot (\dot{\beta} + \dot{\psi}) \,, \tag{4.6}$$

$$F_y = m \cdot \dot{v} \cdot \sin(\beta) + m \cdot v \cdot \cos(\beta) \cdot (\dot{\beta} + \dot{\psi}) \,, \tag{4.7}$$

where $\dot{\psi} = r$ is derivation of yaw angle that was not negleted (via assumptions above) and so needs to be included.
The last equation is for self-aligning torque around vertical z-axis:

$$J \cdot \ddot{\psi} = M_z \,, \tag{4.8}$$

where J is moment of inertia and M_z is moment acting around the z-axis. To get forces acting on the front and rear wheel, the coordinate tranformation was used. From picture [4.2] is clear that forces F_x and F_y are sum of forces acting on the rear and front wheels

(e.g., F_{xf}, F_{xr} and F_{yf}, F_{yr} respectively) where forces on the wheels are rotated by steering angles δ_f and δ_r using rotational matrices as:

$$\begin{bmatrix} F_x \\ F_y \end{bmatrix} = \begin{bmatrix} \cos(\delta_f) & -\sin(\delta_f) \\ \sin(\delta_f) & \cos(\delta_f) \end{bmatrix} \cdot \begin{bmatrix} F_{xf} \\ F_{yf} \end{bmatrix} + \begin{bmatrix} \cos(\delta_r) & -\sin(\delta_r) \\ \sin(\delta_r) & \cos(\delta_r) \end{bmatrix} \cdot \begin{bmatrix} F_{xr} \\ F_{yr} \end{bmatrix} . \tag{4.9}$$

The moment M_z is dependent on F_y where the front wheel has δ_f angle aligned with the direction of $\dot{\psi}$ and the rear wheel has δ_r not because it's direction is opposite to $\dot{\psi}$ as seen in [4.2].

$$M_z = l_f \cdot \sin(\delta_f) \cdot F_{xf} + l_f \cdot \cos(\delta_f) \cdot F_{yf} - l_r \cdot \sin(\delta_r) \cdot F_{xr} - l_r \cdot \cos(\delta_r) \cdot F_{yr} \ , \tag{4.10}$$

where l_f is distance between front axle and CG and l_r is distance between rear axle and CG.

4.1.2 Tyre slip angles

Tyre slip angles are defined as angle between velocity vector to given axle coordinate system of F_{xf} and F_{yf} for the front wheel as

$$\alpha_f = \arctan\left(\frac{v_{yf}}{v_{xf}}\right) \ , \tag{4.11}$$

where v_{xf} and v_{yf} are components of velocity vector v_f which is indicating direction and velocity of the front wheel. These components can be translated to vehicles coordinate system using the following coordinate transformation

$$\begin{bmatrix} v_x \\ v_y \end{bmatrix} = \begin{bmatrix} \cos(\delta_f) & -\sin(\delta_f) \\ \sin(\delta_f) & \cos(\delta_f) \end{bmatrix} \cdot \begin{bmatrix} v_{xf} \\ v_{yf} \end{bmatrix} . \tag{4.12}$$

Rotational matrix is orthogonal and so it's inverse is it's transpose and with

$$v_x = v \cdot \cos(\beta) \ , \tag{4.13}$$

$$v_y = v \cdot \sin(\beta) + l_f \cdot \dot{\psi} \ , \tag{4.14}$$

where a member $l_f \cdot \dot{\psi}$ is on account of yaw rate influence on lateral velocity, implying

$$\begin{bmatrix} v_{xf} \\ v_{yf} \end{bmatrix} = \begin{bmatrix} \cos(\delta_f) & \sin(\delta_f) \\ -\sin(\delta_f) & \cos(\delta_f) \end{bmatrix} \cdot \begin{bmatrix} v \cdot \cos(\beta) \\ v \cdot \sin(\beta) + l_f \cdot \dot{\psi} \end{bmatrix} . \tag{4.15}$$

The same process applies for the rear tyre slip angle α_r but member $l_r \cdot \dot{\psi}$ has to be subtracted (via picture [4.2]). Finally, the following equations are derived

$$\alpha_f = -\arctan\left(\frac{(v \cdot \sin(\beta) + l_f \cdot \dot{\psi}) \cdot \cos(\delta_f) - v \cdot \cos(\beta) \cdot \sin(\delta_f)}{|(v \cdot \sin(\beta) + l_f \cdot \dot{\psi}) \cdot \sin(\delta_f) + v \cdot \cos(\beta) \cdot \cos(\delta_f))|}\right) , \tag{4.16}$$

$$\alpha_r = -\arctan\left(\frac{(v \cdot \sin(\beta) - l_r \cdot \dot{\psi}) \cdot \cos(\delta_r) - v \cdot \cos(\beta) \cdot \sin(\delta_r)}{|(v \cdot \sin(\beta) - l_r \cdot \dot{\psi}) \cdot \sin(\delta_r) + v \cdot \cos(\beta) \cdot \cos(\delta_r))|}\right) , \tag{4.17}$$

where absolute value in the denominator is present to handle singularities. Now, with (4.16) and (4.17) lateral forces acting on the wheels can be calculated using Pacejka Magic Formula.

4.1.3 Slip ratios

The formula for slip ratios is adopted from [7]. Slip ratios are depicted as difference between v_{xf} (defined above) of the vehicle and circumferential velocity v_{cf} of a tyre for the front axle. Circumferential velocity is calculated as

$$v_{cf} = \omega_f \cdot R_f , \tag{4.18}$$

where ω_f is angular velocity of a given wheel and R_i is its radius. The same goes for the rear wheel. With that, slip ratios are defined as follows

$$\lambda_f = \frac{v_{cf} - v_{xf}}{\max(|v_{cf}|, |v_{xf}|)} , \tag{4.19}$$

$$\lambda_r = \frac{v_{cr} - v_{xr}}{\max(|v_{cr}|, |v_{xr}|)} , \tag{4.20}$$

$$-1 \leq \lambda_i \leq 1 , \tag{4.21}$$

where absolute value is present to ensure that denominator will normalize numerator. Also, λ_i cannot be smaller than -1 or bigger than 1 (via condition (4.21)).

4.1.4 Wheel angular velocity

For enumeration of angular velocities ω_f and ω_r, the formula of it's angular acceleration from [2] is chosen

$$J_f \cdot \dot{\omega}_f = \tau_f - R_f \cdot F_{xf} - \text{sign}(\omega_f) \cdot \tau_{Bf} - k_f \cdot v_{xf} , \tag{4.22}$$

$$J_r \cdot \dot{\omega}_r = \tau_r - R_r \cdot F_{xr} - \text{sign}(\omega_r) \cdot \tau_{Br} - k_r \cdot v_{xr} , \tag{4.23}$$

where J_f and J_r are moments of inertia of respected wheel around its y-axis, k_f and k_r are coefficients of road drag for the given wheel, τ_f and τ_r are drive torques applied by drivetrain on the given wheel and τ_{Bf} and τ_{Br} are brake torques applied by brakes on the given wheel. Member $k_i \cdot v_{xi}$ has been added for account of dissipative force acting on the wheel.

4.1.5 Tyre dynamics

This section is going throught calculation of F_{xf}, F_{xr}, F_{yf} and F_{yr}. It is one of the most important aspects of the model and so there are many kinds of calculations. The comparison of such techniques can be found in [7]. Pacejka Magic Formula is taken from [6] and calculates all torques and forces acting on the tyre. For simplification, the simplified Pacejka Magic Formula is used which has less coefficients and is easier to understand and manage.

4.1.5.1 Simplified Pacejka Magic Formula

Simplified Pacejka Magic Formula has only one formula

$$F_{xi,yi}(\theta_i) = F_{zi} \cdot D \cdot \sin(C \cdot \arctan(B \cdot \theta_i - E \cdot (B \cdot \theta_i - \arctan(B \cdot \theta_i)))) \ , \qquad (4.24)$$

where i represents both front and rear, θ_i is α_i, when computing lateral forces F_{yf} and F_{yr}, and λ_i, when calculating longitudinal forces F_{xf} and F_{xr}, and F_{zi} is force of the load acting on given wheel. The form of $F_{xi,yi}$ curve across different θ_i values is dependent on coefficients:

- D = peak value of the curve,
- C = shape of peak value,
- B = stiffness,
- E = curvature.

The values, that were used, are in table [4.2] and [4.1] for angles θ_i in radians where i stands for rear and front. The reason for slightly different coefficients between calculating of the rear and front wheel lateral forces is for change of understeering and oversteering behavior of the car (see more in chapter [**Influence of Pacejka coefficients on behavior of a vehicle**]). The curves of individual lateral and longitudinal forces for the front and the rear are depicted below for given vertical load forces F_{zi} where wheel load force $F_{zf} = 5297$ N and $F_{zr} = 6377$ N is used in the model.

	F_{xi}	F_{yf}	F_{yr}
D	1	1	1
C	1.4	1.45	1.35
B	4	10	9
E	0.1	0.1	0.1

Table 4.1: Used coefficients for simplified Pacejka Magic Formula for the oversteering behavior of the car

	F_{xi}	F_{yf}	F_{yr}
D	1	1	1
C	1.4	1.45	1.55
B	4	10	12
E	0.1	0.1	0.15

Table 4.2: Used coefficients for simplified Pacejka Magic Formula for the understeering behavior of the car

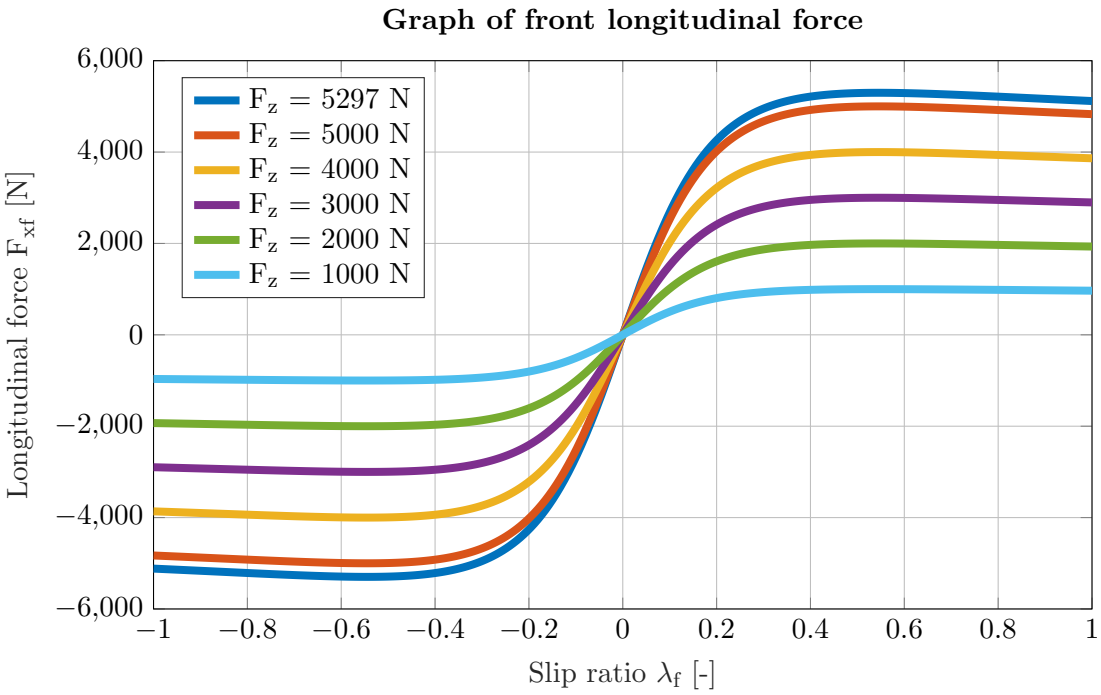

Figure 4.3: Longitudinal force F_{xf} dependent on slip ratio λ_f computed by simplified Pacejka Magic formula with coefficients from [4.2]

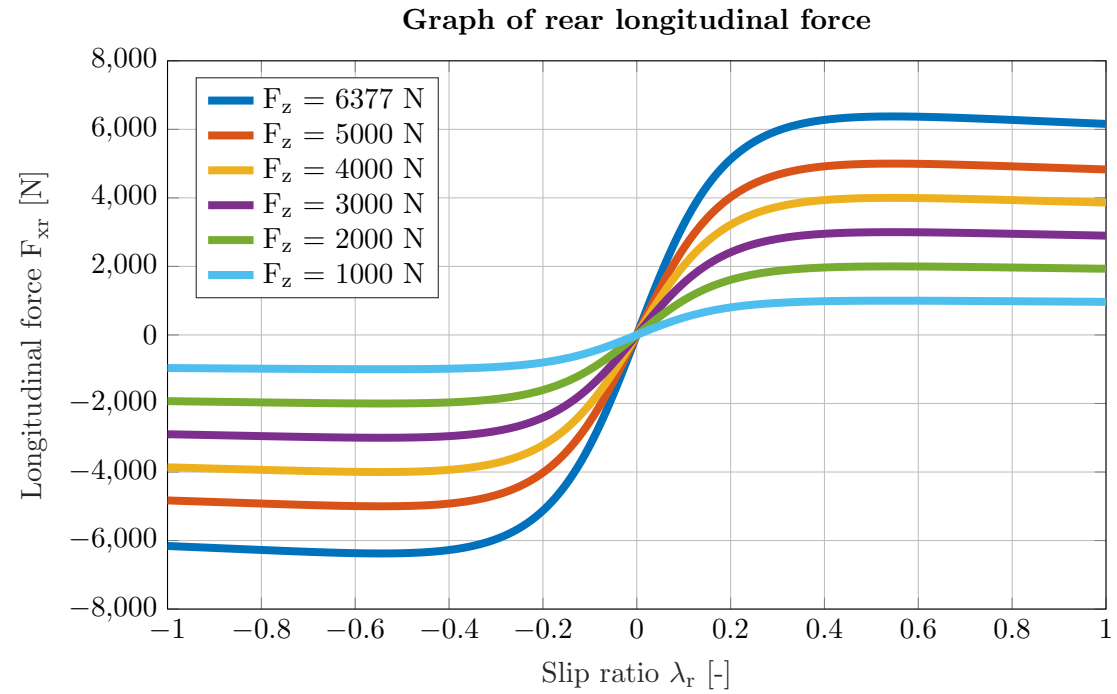

Figure 4.4: Longitudinal force F_{xr} dependent on slip ratio λ_r computed by simplified Pacejka Magic formula with coefficients from [4.2]

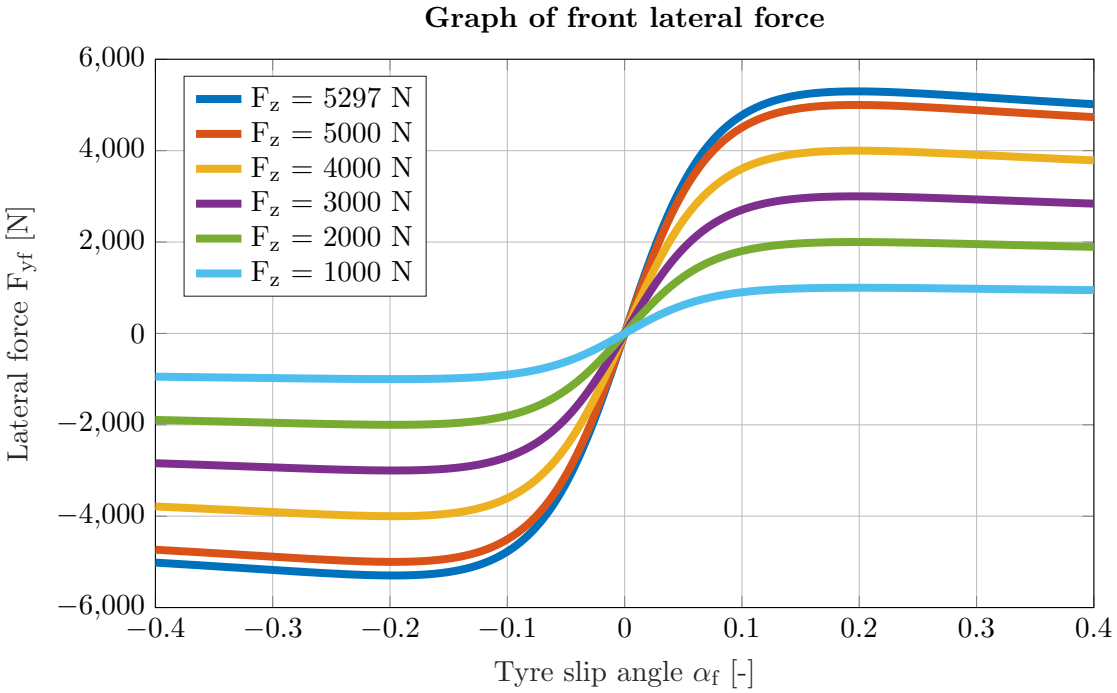

Figure 4.5: Lateral force F_{yf} dependent on tyre slip angle α_r computed by simplified Pacejka Magic formula with coefficients from [4.2]

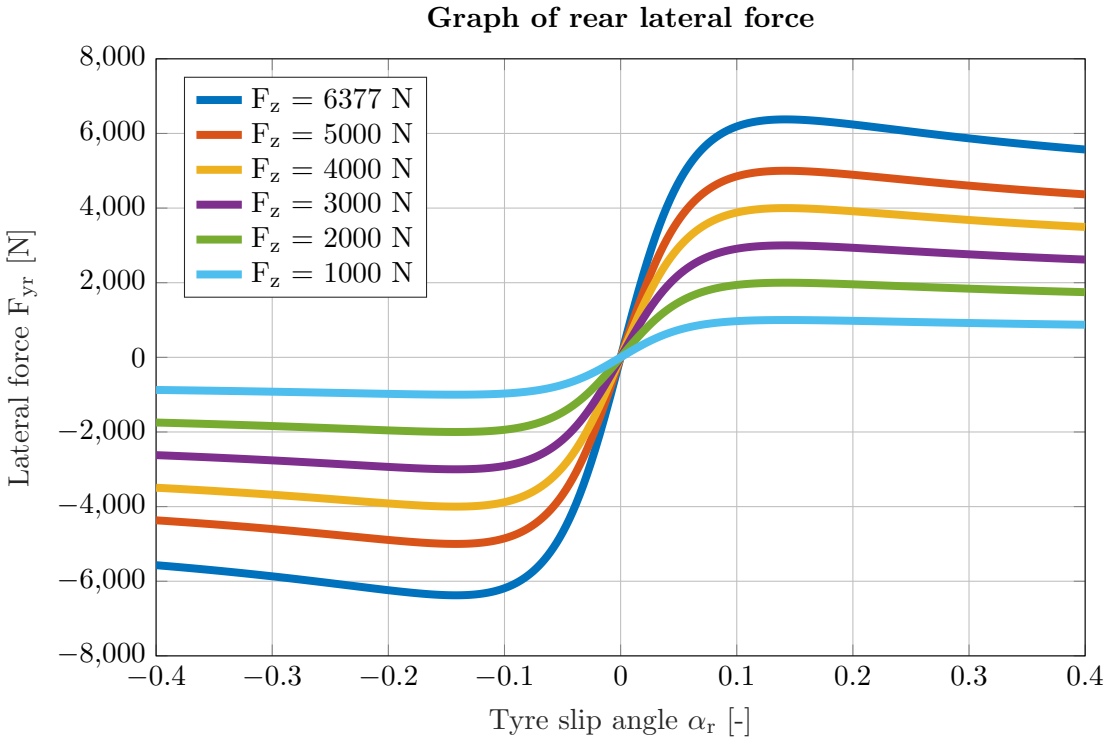

(a) The understeering behavior of the car

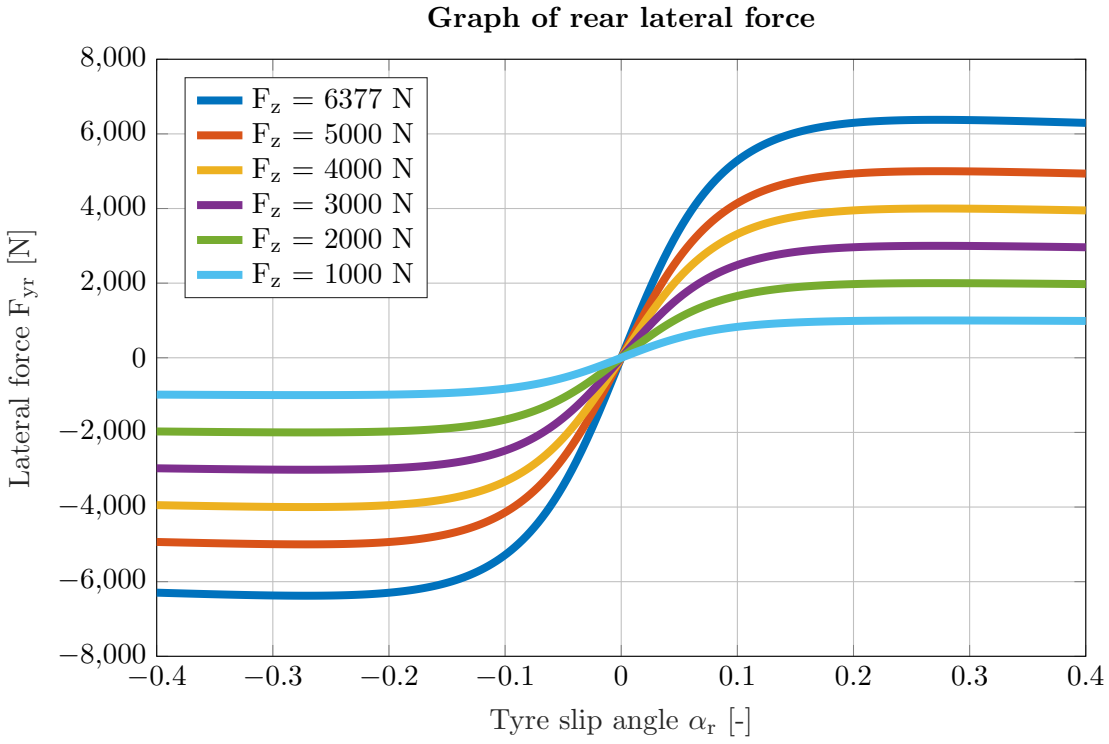

(b) The oversteering behavior of the car

Figure 4.6: Lateral force F_{yr} dependent on tyre slip angle α_r computed by simplified Pacejka Magic formula with coefficients from [4.2] and [4.1]

4.1.5.2 Traction ellipse

Forces F_x and F_y should not be greater than wheel-load force F_{zi} acting on the given wheel. However, Pacejka Magic Formula has not got such condition and so traction ellipse is used (also friction ellipse) to scale computed forces. This idea is explained in formula

$$\sqrt{\frac{F_{xf}^2}{D_x^2} + \frac{F_{yf}^2}{D_y^2}} = \mu \cdot F_{zf} \ , \tag{4.25}$$

$$\sqrt{\frac{F_{xr}^2}{D_x^2} + \frac{F_{yr}^2}{D_y^2}} = \mu \cdot F_{zr} \ , \tag{4.26}$$

where D_x is coeffient for calculating force F_{xi} and D_y is coeffient for calculating force F_{yi} in simplified Pacejka Magic Formula in table [4.2] and μ is friction coefficient between road and tyre, and in picture [4.7] below.

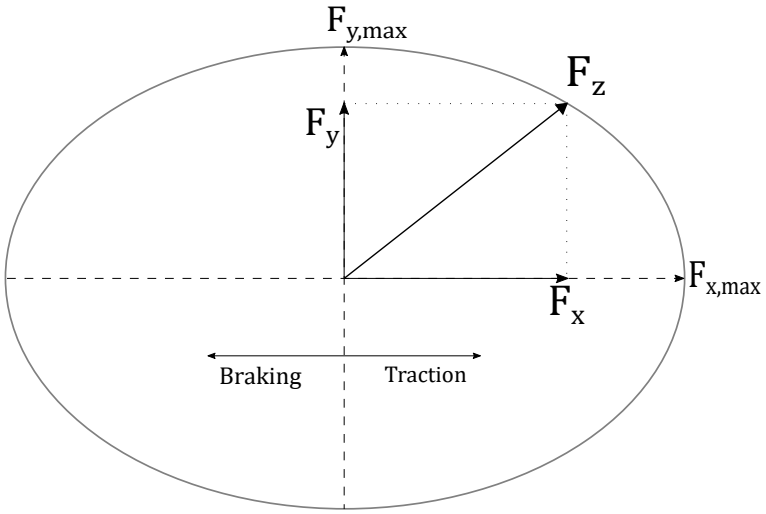

Figure 4.7: Graphical interpretation of traction ellipse

The scaling method is adopted from [7]

$$\gamma = \arccos\left(\frac{|\lambda_i|}{\sqrt{\lambda_i^2 + \sin(\alpha_i)^2}}\right) \ , \tag{4.27}$$

$$\mu_{xi,act} = \frac{F_{xi,max}}{F_{zi}} \ , \quad \mu_{yi,act} = \frac{F_{yi,max}}{F_{zi}} \ , \tag{4.28}$$

$$\mu_{xi,max} = D_x \ , \quad \mu_{yi,max} = D_y \ , \tag{4.29}$$

$$\mu_x = \frac{1}{\sqrt{\mu_{x,act}^{-2} + \left(\frac{\tan(\gamma)}{\mu_{y,max}}\right)^2}} \ , \quad F_{xi} = \left|\frac{\mu_x}{\mu_{x,act}}\right| \cdot F_{xi,max} \ , \tag{4.30}$$

$$\mu_y = \frac{\tan(\gamma)}{\sqrt{\mu_{x,max}^{-2} + \left(\frac{\tan(\gamma)}{\mu_{y,act}}\right)^2}} \ , \quad F_{yi} = \left|\frac{\mu_y}{\mu_{y,act}}\right| \cdot F_{yi,max} \ , \tag{4.31}$$

where i stands for front and rear, λ_i are slip ratios and α_i are tyre slip angles from respected wheel. The forces $F_{xi,max}$ and $F_{yi,max}$ are directly taken from formula (4.24).

4.1.6 Linearized model

Here, linerarized form of nonlinear equations above is derived. First, angles δ_f, δ_r and β are assumed to be small which entail following

$$\sin(x) \approx x \ , \qquad \cos(x) \approx 1 \ , \tag{4.32}$$

where their linear approximation around 0 is used. Then, the usage on (4.6), (4.7) and (4.8) is implying

$$F_x = m \cdot \dot{v} - m \cdot v \cdot \beta \cdot (\dot{\beta} + \dot{\psi}) \ , \tag{4.33}$$

$$F_y = m \cdot \dot{v} \cdot \beta - m \cdot v \cdot (\dot{\beta} + \dot{\psi}) \ , \tag{4.34}$$

$$M_z = J \cdot \ddot{\psi} \ . \tag{4.35}$$

Next, the velocity is assumed to be constant $\dot{v} = 0$. With that, formulas (4.33) and (4.34) imply $F_x = -\beta \cdot F_y$. Moreover, with condition $\beta^2 \ll 1$:

$$F_y = m \cdot v \cdot (\dot{\beta} + \dot{\psi}) \ , \tag{4.36}$$

$$M_z = J \cdot \ddot{\psi} \ . \tag{4.37}$$

With linearization of tyre slip angles (4.16) and (4.17) is derived as in [7]

$$\alpha_f = \delta_f - \beta - \frac{l_f}{v} \cdot r \ , \tag{4.38}$$

$$\alpha_r = \delta_r - \beta + \frac{l_r}{v} \cdot r \ , \tag{4.39}$$

where $r = \dot{\psi}$. Now, force F_y and torque M_z is going to be derived. Nonlinear forces of F_{yf} and F_{yr} can be linearized by constant named cornering stiffness c_r and c_f respectively

$$F_{yf} = c_f \cdot \alpha_f \ , \tag{4.40}$$

$$F_{yr} = c_r \cdot \alpha_r \ , \tag{4.41}$$

where $F_y = F_{yf} + F_{yr}$. Because of the fact that the car goes with constant velocity with small steering angles, the following simplifications can be applied

$$F_{xf} \cdot \delta_f \approx 0 \ , \tag{4.42}$$

$$F_{xr} \cdot \delta_r \approx 0 \ , \tag{4.43}$$

what with (4.9) and (4.10) gives following

$$F_y = c_f \cdot \alpha_f + c_r \cdot \alpha_r = c_f \cdot \delta_f - c_f \cdot \beta - c_f \cdot \frac{l_f}{v} \cdot r + c_r \cdot \delta_r - c_r \cdot \beta + c_r \cdot \frac{l_r}{v} \cdot r \ , \tag{4.44}$$

which equals to $F_y = F_{yf} + F_{yr}$. The same goes for torque

$$M_z = l_f \cdot c_f \cdot \alpha_f - l_r \cdot c_r \cdot \alpha_r \ . \tag{4.45}$$

Finally, the final differential equations are written down as:

$$\dot{\beta} = -\frac{c_f + c_r}{m \cdot v} \cdot \beta + \left(\frac{l_r \cdot c_r - l_f \cdot c_f}{m \cdot v^2} - 1 \right) \cdot r + \frac{c_f}{m \cdot v} \cdot \delta_f + \frac{c_r}{m \cdot v} \cdot \delta_r \ , \tag{4.46}$$

$$\dot{r} = \frac{l_r \cdot c_r - l_f \cdot c_f}{J} \cdot \beta - \frac{l_f^2 \cdot c_f + l_r^2 \cdot c_r}{J \cdot v} \cdot r + \frac{l_f \cdot c_f}{J} \cdot \delta_f - \frac{l_r \cdot c_r}{J} \cdot \delta_r \ , \tag{4.47}$$

which in state-space form is equal to:

$$\begin{bmatrix} \dot{\beta} \\ \dot{r} \end{bmatrix} = \begin{bmatrix} -\frac{c_f + c_r}{m \cdot v} & \frac{l_r \cdot c_r - l_f \cdot c_f}{m \cdot v^2} - 1 \\ \frac{l_r \cdot c_r - l_f \cdot c_f}{J} & -\frac{l_f^2 \cdot c_f + l_r^2 \cdot c_r}{J \cdot v} \end{bmatrix} \cdot \begin{bmatrix} \beta \\ r \end{bmatrix} + \begin{bmatrix} \frac{c_f}{m \cdot v} & \frac{c_r}{m \cdot v} \\ \frac{l_f \cdot c_f}{J} & -\frac{l_r \cdot c_r}{J} \end{bmatrix} \cdot \begin{bmatrix} \delta_f \\ \delta_r \end{bmatrix} . \tag{4.48}$$

4.2 Twin-track

All controllers are modeled on single-track system above. However, testing was done mainly on the twin-track model provided by Bc. Vít Cibulka and Ing. Denis Efremov from Faculty of Electrical Enegineering and so here only the differences with a single-track model are listed.

4.2.1 States

The model is based on [2]. System itself have mainly 6 coordinate systems (CS). Inertial earth-fixed and body-fixed in CG coordinate systems with 4 more for each wheel. There are 16 states that include 3 for position of vehicle s in earth-fixed CS, 3 for velocity of the car v in body fixed CS, 3 angular velocities of body of the vehicle ω in body-fixed CS, 3 Euler angles ϕ, θ, ψ of earth-fixed CS and 4 wheel's angular velocities in each wheel's CS respectively.

4.2.2 Tyre dynamics

Tyre dynamics were used the same as in [4.1.5].

4.2.3 Slip angles and ratios

Slip ratios are enumerated using the same equations but input velocities and tyre slip angles are calculated in slightly different manner. For more detail see [2].

4.2.4 Wheel angular velocity

Wheel angular velocity is calculated like in [4.1.4] but the motor power and maximum torque are limited.

5. Robust decoupling

5.1 Model

This method is taken from [1] and was written by Jürger Ackermann. Presented system is diveded into two: controller and steering dymamics. For steering dynamics single-track model derived above is used. The controller is formed by three control laws:

$$\dot{\delta_f} = w_f - r \ , \tag{5.1}$$

$$w_f = k_S \cdot (a_{fref} - a_f) + \frac{1}{v} \cdot a_f \ , \tag{5.2}$$

$$\delta_r = \left(k_D - \frac{l}{v} \right) \cdot r + w_r \ , \tag{5.3}$$

where δ_f is steering angle for the front wheel and δ_r for the rear wheel, $l = l_f + l_r$ where l_f is a distance of CG to the front axle and l_r is s distance of CG to the rear axle, $r = \dot{\psi}$ is yaw rate, v is velocity, a_f is lateral accleration of the front axle and a_{fref} is referenced lateral accleration for the front axle, k_S and k_D are tunable constants and w_f and w_r are residual variables.

5.1.1 First control law

Formula (5.1) removes dependency of side slip angle β and of $\alpha_f = \delta_f - \beta - \frac{l_f \cdot r}{v}$ on yaw rate r. With that, the controller is robust. Variable a_{fref} is chosen as reference. It is possible to calculate it directly from angle δ_S from steering wheel with velocity dependent gain $k_f(v)$ as

$$a_{fref}(t) = k_f(v) \cdot \delta_S(t) \ , \tag{5.4}$$

where

$$k_f(v) = \frac{l \cdot c_f \cdot c_r \cdot v^2}{c_f \cdot c_r \cdot l^2 + m \cdot v^2 \cdot (c_r \cdot l_r - c_f \cdot l_f)} \ , \tag{5.5}$$

where c_f and c_r are linerized cornernering stiffness coefficients of given wheels.

5.1.2 Second control law

Formula (5.2) removes dependency of tyre slip angle α_f on velocity v. The non-linear influence of F_{yf} and m can be tuned by high enough gain of k_S. Ackermann suggests value

$$k_S = 30 \cdot \frac{m \cdot l_r}{c_f \cdot l} \ , \tag{5.6}$$

because of limitations that human driver is restricted by, where m is mass of the vehicle and c_f is cornering stiffness coefficient of linerized system for front wheel.

5.1.3 Third control law

Formula (5.3) defines yaw rate damper dependent on velocity v. Constant k_D is varying yaw rate damping variable. The w_r variable is chosen to make the side slip angle β the smallest and so it helps maneuverability of the car:

$$w_r(s) = F_r(s, v) \cdot a_{fref}(s) \ , \tag{5.7}$$

where $F_r(s, v)$ is transfer function described below

$$F_r(s, v) = k_r(v) \cdot \frac{1 + T_0(s) \cdot s}{[1 + T_1(s) \cdot s] \cdot [1 + T_2(s) \cdot s]} \ , \tag{5.8}$$

where

$$k_r(v) = \frac{m \cdot l_f \cdot v^2 - k_D \cdot l \cdot c_r \cdot v + l \cdot l_f \cdot c_r}{c_r \cdot v^2 \cdot l} \ , \tag{5.9}$$

$$T_0(v) = \frac{-m \cdot l_r \cdot l_f \cdot v}{m \cdot l_f \cdot v^2 - k_D \cdot l \cdot c_r \cdot v + l \cdot l_f \cdot c_r} \ , \tag{5.10}$$

$$T_1(w) = \frac{m \cdot l_r}{k_S \cdot c_f \cdot l} \ , \tag{5.11}$$

$$T_2(v) = \frac{l_f}{v} \ . \tag{5.12}$$

5.2 Method derivation

Now, the controller with equations from [**Robust decoupling**] by approach used in [1] shall be derived. Firstly, the first control law in (5.1) is proven. By derivation of

$$\alpha_f = \delta_f - \beta - \frac{l_f}{v} \cdot r \tag{5.13}$$

with assumption that velocity is not time-variant and thus constant

$$\dot{\alpha}_f = \dot{\delta}_f - \dot{\beta} - \frac{l_f}{v} \cdot \dot{r} = w_f - r - \frac{c_f}{m \cdot v} \cdot \alpha_f - \frac{c_r}{m \cdot v} \cdot \alpha_r - \frac{l_f^2 \cdot c_f}{v \cdot J} \cdot \alpha_f + \frac{l_f \cdot c_r \cdot l_r}{v \cdot J} \cdot \alpha_r \ , \tag{5.14}$$

which with simplification of $J = m \cdot l_f \cdot l_r$ equals to

$$\dot{\alpha}_f = w_f - \frac{c_f}{m \cdot v} \cdot \left(\frac{l_f}{l_r} + 1 \right) \cdot \alpha_f \ , \tag{5.15}$$

where $\frac{1}{l_r}$ is extracted from brackets and simplifying (5.15) with $l = l_f + l_r$ gives

$$\dot{\alpha}_f = w_f - \frac{c_f \cdot l}{m \cdot v \cdot l_r} \cdot \alpha_f \ , \tag{5.16}$$

which is not directly dependent on yaw rate r or steering angles δ_f and δ_r.

Next, the second control law in (5.2) is proven. The front axle lateral acceleration

is by second Newton law equals to

$$a_f = \frac{1}{m_f} \cdot F_{yf}(\alpha_f) = \frac{l}{m \cdot l_r} \cdot F_{yf} = \frac{l \cdot c_f}{m \cdot l_r} \cdot \alpha_f \ . \tag{5.17}$$

The substituting of (5.17) into formula (5.2) implies

$$w_f = k_S \cdot a_{fref} - \frac{k_S \cdot l \cdot c_f}{m \cdot l_r} \cdot \alpha_f + \frac{l \cdot c_f}{v \cdot m \cdot l_r} \cdot \alpha_f \tag{5.18}$$

and by substituting it into (5.16)

$$\dot{\alpha}_f = k_S \cdot a_{fref} - \frac{k_S \cdot c_f \cdot l}{m \cdot l_r} \cdot \alpha_f + \frac{c_f \cdot l}{v \cdot m \cdot l_r} \cdot \alpha_f - \frac{c_f \cdot l}{m \cdot v \cdot l_r} \cdot \alpha_f \ , \tag{5.19}$$

which is velocity independent.

Lastly, the controller and model is described by differential equations with non-linerized tyre slip angles as

$$\begin{bmatrix} \dot{\beta} \\ \dot{r} \\ \dot{\delta}_f \end{bmatrix} = \begin{bmatrix} \frac{c_f}{m \cdot v} & \frac{c_r}{m \cdot v} & -1 \\ \frac{c_f \cdot l_f}{J} & -\frac{c_r \cdot l_r}{J} & 0 \\ \frac{(1/v - k_S) \cdot l}{m \cdot l_r} & 0 & -1 \end{bmatrix} \cdot \begin{bmatrix} \alpha_f \\ \alpha_r \\ r \end{bmatrix} + \begin{bmatrix} 0 \\ 0 \\ k_S \end{bmatrix} \cdot a_{fref} \ , \tag{5.20}$$

where formulas (4.36), (4.37), (4.44) and (4.45) and $J = m \cdot l_f \cdot l_r$ were used. The rotational dynamics is subsystem of (5.20) formed by $\dot{r}$ and $\dot{\delta}_f$. The tyre slip angle α_f is expressed by (5.19) and so only α_r has been linearized by formula $\alpha_r = \delta_r - \delta_f + \alpha_f + \frac{l}{v} \cdot r$ to obtain

$$\begin{bmatrix} \dot{r} \\ \dot{\delta}_f \end{bmatrix} = \begin{bmatrix} -\frac{c_r \cdot l}{v \cdot m \cdot l_r} & \frac{c_r}{m \cdot l_f} \\ -1 & 0 \end{bmatrix} \cdot \begin{bmatrix} r \\ \delta_f \end{bmatrix} - \begin{bmatrix} \frac{c_r}{m \cdot l_f} \\ 0 \end{bmatrix} \cdot \delta_r + d_s(\alpha_f) \ , \tag{5.21}$$

where d_s is the remainder (input from the subsystem)

$$d_s = \begin{bmatrix} -\frac{c_r}{m \cdot l_f} + \frac{c_f}{m \cdot l_r} \\ \frac{c_f \cdot (1/v - k_S) \cdot l}{m \cdot l_r} \end{bmatrix} \cdot \alpha_f + \begin{bmatrix} 0 \\ k_S \end{bmatrix} \cdot a_{fref} \ . \tag{5.22}$$

The damping can be computed from (5.21) with characteristic polynomial to be velocity dependent as

$$D = \frac{l}{2 \cdot v} \ . \tag{5.23}$$

Therefore, the third control law (5.3) swaps $\frac{l}{v}$ to k_D by substracting it. The effect can be seen in (5.21) where δ_r was substituded with (5.3).

Finally, the whole linearized system can be described by 5 differential equations in

a state-space form as

$$\begin{bmatrix} \dot{\beta} \\ \dot{r} \\ \dot{\delta}_f \\ \dot{\delta}_x \\ \dot{\delta}_r \end{bmatrix} = \begin{bmatrix} -\frac{c_f + c_r}{m \cdot v} & \frac{l_r \cdot c_r - l_f \cdot c_f}{m \cdot v^2} - 1 & \dots \\ \frac{l_r \cdot c_r - l_f \cdot c_f}{J} & -\frac{l_f^2 \cdot c_f + l_r^2 \cdot c_r}{v \cdot J} & \dots \\ \frac{c_f \cdot (l_f + l_r) \cdot (-k_S + 1/v)}{m \cdot v} & \frac{c_f \cdot (l_f + l_r) \cdot l_f \cdot (-k_S + 1/v)}{m \cdot v^2} - 1 & \dots \\ 0 & 0 & \dots \\ 0 & 0 & \dots \end{bmatrix}$$

$$\begin{bmatrix} \frac{c_f}{m \cdot v} & 0 & \frac{c_r}{m \cdot v} \\ \frac{l_f \cdot c_f}{J} & 0 & -\frac{l_r \cdot c_r}{J} \\ \frac{c_f \cdot (l_f + l_r) \cdot (-k_S + 1/v)}{m \cdot v} & 0 & 0 \\ 0 & -T_3(v)/T_4(v) & -1 \\ 0 & 1/T_4(v) & 0 \end{bmatrix} \cdot \begin{bmatrix} \beta \\ r \\ \delta_f \\ \delta_x \\ \delta_r \end{bmatrix} \quad , \quad (5.24)$$

$$+ \begin{bmatrix} 0 \\ 0 \\ k_S \\ k_r(v) - k_r(v) \cdot T_0(v) \cdot T_3(v)/T_4(v) \\ T_0(v) \cdot k_r(v)/T_4(v) \end{bmatrix} \cdot a_{fref}$$

where

$$T_3(v) = T_1 + T_2(v) \ , \quad (5.25)$$

$$T_4(v) = T_1 \cdot T_2(v) \ , \quad (5.26)$$

$$\delta_x = T_4(v) \cdot \dot{\delta}_r - T_0(v) \cdot k_r(v) \cdot a_{fref} \quad (5.27)$$

are defined in equations (5.9), (5.10), (5.11) and (5.12).

6. Rear wheel steer angle control system

6.1 Model

This method is taken from [4]. It uses imaginary position of a point X on the car axis to maneuver vehicle around. The front steering angle δ_f is unchanged. The focus is on computation of δ_r from δ_f. The controller is derived with the same approach as in [4] but using linearized equations of single-track model derived above. When l_3 is the distance from CG to point X then lateral velocity in X is equal to:

$$v_{Xy} = v_y - l_3 \cdot r \ . \tag{6.1}$$

The feedforward works in such a way that keeps condition $v_{Xy} = 0 \ \mathrm{m \cdot s^{-1}}$ which implies that v_y of CG can be defined as:

$$v_y = l_3 \cdot r \ . \tag{6.2}$$

The form of the final transfer function is

$$G(s) = \frac{\delta_r}{\delta_f} = \frac{K(v) + T_1(v) \cdot s}{1 + T_2(v) \cdot s} \ , \tag{6.3}$$

where

$$K(v) = \frac{c_f \cdot (m \cdot v^2 \cdot l_f + c_r \cdot l \cdot (l_3 - l_r))}{c_r \cdot (m \cdot v^2 \cdot l_r + c_f \cdot l \cdot (l_3 + l_f))} \ , \tag{6.4}$$

$$T_1(v) = \frac{c_f \cdot v \cdot (m \cdot l_f \cdot l_3 - J)}{c_r \cdot (m \cdot v^2 \cdot l_r + c_f \cdot l \cdot (l_3 + l_f))} \ , \tag{6.5}$$

$$T_2(v) = \frac{v \cdot (m \cdot l_r \cdot l_3 + J)}{m \cdot v^2 \cdot l_r + c_f \cdot l \cdot (l_3 + l_f)} \ . \tag{6.6}$$

6.2 Method derivation

Formula (6.2) is inserted into (4.36), (4.44) and (4.45) where linearized form of side slip angle $\beta = \sin\left(\frac{v_y}{v}\right) \approx \frac{v_y}{v}$ and assumption that $\dot{v} = 0$ are used, which [4] did not include, to get

$$F_y = m \cdot v \cdot (\dot{\beta} + r) \ , \tag{6.7}$$

$$F_y = c_f \cdot \delta_f - c_f \cdot \frac{l_3}{v} \cdot r - c_f \cdot \frac{l_f}{v} \cdot r + c_r \cdot \delta_r - c_r \cdot \frac{l_3}{v} \cdot r + c_r \cdot \frac{l_r}{v} \cdot r \ , \tag{6.8}$$

$$\begin{aligned} J \cdot \dot{r} = {} & l_f \cdot c_f \cdot \delta_f - l_f \cdot c_f \cdot \frac{l_3}{v} \cdot r - l_f \cdot c_f \cdot \frac{l_f}{v} \cdot r \\ & + l_r \cdot c_r \cdot \delta_r - l_r \cdot c_r \cdot \frac{l_3}{v} \cdot r + l_r \cdot c_r \cdot \frac{l_r}{v} \cdot r \ . \end{aligned} \tag{6.9}$$

Here, δ_r is assumed that it can be described as $\delta_r = G(s) \cdot \delta_f$ and using Laplace tranform the following simplifications can be obtained: $\dot{\beta} \approx s \cdot \beta$ and $\dot{r} \approx s \cdot r$. Simple algebraic adjustments give

$$r \cdot \left(s \cdot m \cdot l_3 + m \cdot v + c_f \cdot \frac{l_3}{v} + c_f \cdot \frac{l_f}{v} + c_r \cdot \frac{l_3}{v} - c_r \cdot \frac{l_r}{v} \right) = (c_f + c_r \cdot G(s)) \cdot \delta_f \ , \tag{6.10}$$

$$r \cdot \left(s \cdot J + m \cdot v + c_f \cdot l_f \cdot \frac{l_3}{v} + c_f \cdot l_f \cdot \frac{l_f}{v} + c_r \cdot l_r \cdot \frac{l_3}{v} - c_r \cdot l_r \cdot \frac{l_r}{v} \right) = (c_f \cdot l_f + c_r \cdot l_r \cdot G(s)) \cdot \delta_f \tag{6.11}$$

and put more simply:

$$A \cdot r = (c_f + c_r \cdot G(s)) \cdot \delta_f \ , \tag{6.12}$$

$$B \cdot r = (c_f \cdot l_f + c_r \cdot l_r \cdot G(s)) \cdot \delta_f \ . \tag{6.13}$$

Now, formula (6.12) has to be equal to (6.13) which can be evalueted with usage of math logic as follows

$$A \cdot (c_f \cdot l_f + c_r \cdot l_r \cdot G(s)) = B \cdot (c_f + c_r \cdot G(s)) \ . \tag{6.14}$$

The solution is

$$G(s) = \frac{l_f \cdot c_f \cdot A - c_f \cdot B}{l_r \cdot c_r \cdot A + c_r \cdot B} \ , \tag{6.15}$$

which is equal to result in [4] but with new assumption that acceleration of vehicle is $\dot{v} = 0$.

6.3 Evaluation

Because there is no feedback from states of the model, controller does not change dynamics of the system but only turning point and so the turning radius stays the same. Therefore, there is no steering but only change up of steering angles according to a given distance l_3 and velocity v. The influence on sign of δ_r can be calculated from

$$\delta_f = \frac{K(v) + T_1(v) \cdot s}{1 + T_2(v) \cdot s} \cdot \delta_f \ , \tag{6.16}$$

where limit $\lim_{s \to 0} G(s) = K(v, l_3)$ is taken. The graph of $K(v, l_3)$ is shown below

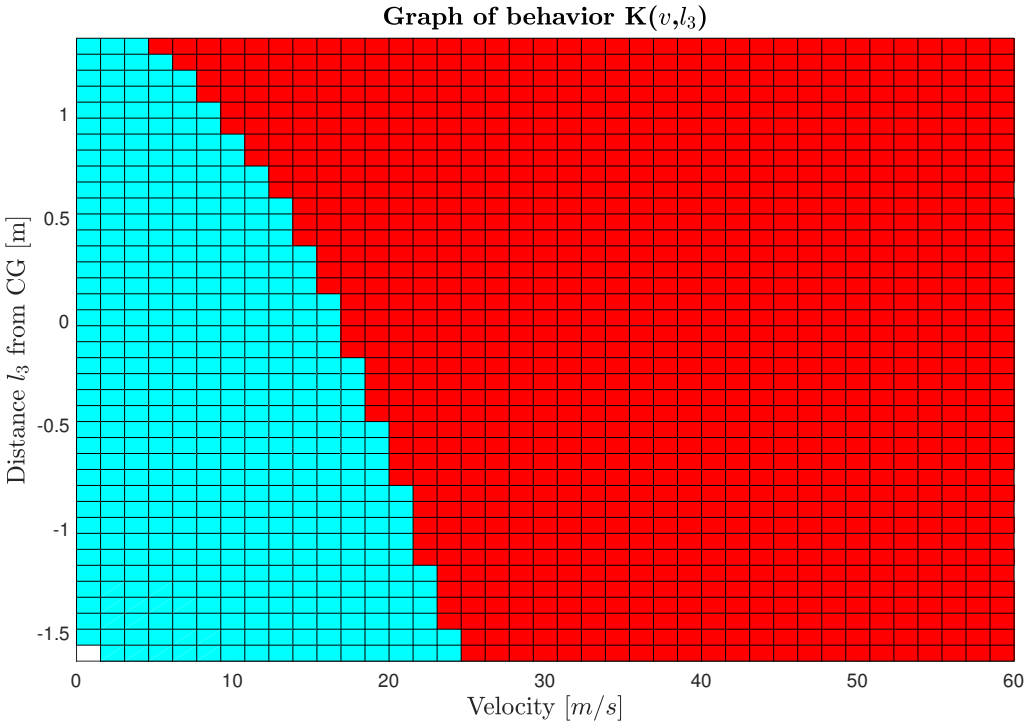

Figure 6.1: Dependency of sign of δ_r on different velocities v and distance l_3 where negative δ_r is in cyan and positive in red for the understeering behavior of the car

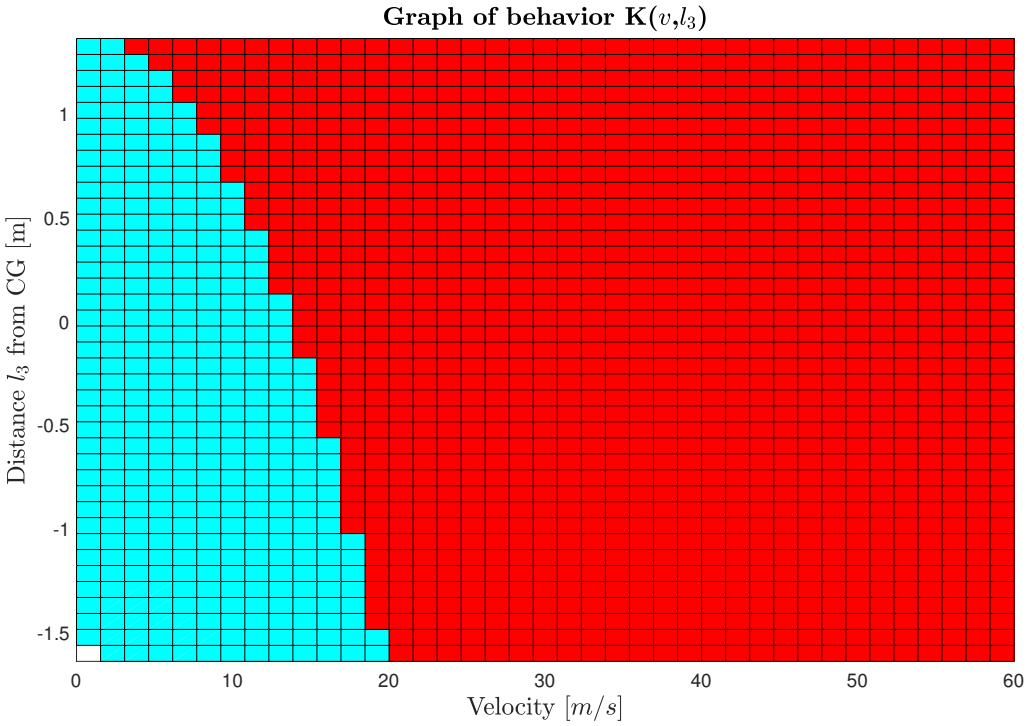

Figure 6.2: Dependency of sign of δ_r on different velocities v and distance l_3 where negative δ_r is in cyan and positive in red for the oversteering behavior of the car

where the distance l_3 is limited from $-l_f$ to l_r. As seen for turning point at front part

of the car, the steering angle δ_r is negative to positive δ_f even for velocities around $20\ \mathrm{m} \cdot \mathrm{s}^{-1}$ and at back part is only around $6\ \mathrm{m} \cdot \mathrm{s}^{-1}$. When the turning point is in the back section of the vehicle, the car tends to oversteer, meaning vehicle steers less than an angle commanded by the driver within the steering wheel range. Because of that, it is desirable only on low velocities. Moreover, the car with negative δ_r to positive δ_f is capable of turning even more than a regular car with only δ_f steering. On the other hand, when the turning point is in the front section, the car tends to understeer, meaning vehicle steers less than angle commanded by the driver within the steering wheel range, and so δ_r can be still negative to positive δ_f on higher velocities helping to turn the car in sharp turns. However, for example, in double lane change maneuver, the positive δ_r is better because it practically enables the car to perform "crab walk" between lanes.

There are several possibilities for feedback control. One is that the controller would change distance l_3 according to a deviation between critical velocity and velocity of the car that would be shifted upward to the desired margin that would be between critical velocity and real velocity of the car. Critical velocity is a value of the velocity in which oversteering vehicle becomes unstable. It can be computed by a formula

$$v_{crit} = (l_f + l_r) \cdot \sqrt{\frac{c_f \cdot c_r}{m \cdot (c_f \cdot l_f - l_r \cdot c_r)}}\ , \tag{6.17}$$

which is derived in [10].

Understeering cars are already stable and so have no critical velocity in compare to oversteering cars. Problem is that the rotational dynamics of the car are not changed, as was mentioned above, and so the critical velocity is independent on a distance l_3. That can be achieved by manually subtracting and adding l_3 to l_f and l_r in controller to calculate new critical velocity. However, the stability of such a system is in question. More in detail is discussed in [**Simlutation ride tests**].

6.4 Proposed control augmentation

The new system has the same transfer function (6.4) but individual parts have a time-variant distance l_3 that is computed using I-controller where $I = 1$ and which reference is critical velocity calculated from the equation $det(A(v) - \lambda) = 0$ which is solved for $Re(\lambda) = 0$ to find stability limit. Here, $A_{3\times3}$ is a state matrix, where the third state is obtained from the transfer function (6.4), and has l_r subtracted from l_3 and l_f increased by l_3. The solution of the equation $det(A(v)) = 0$ is critical velocity which is the reference for I-controller. The control variable is $v^*(t)$. It is calculated by equation $v^* = v + s(v)$ where it is desirable to have value of $s(v)$ low on lower velocities and as high as possible on higher velocities. That is why, an exponential function is used

$$s(v) = 100 - 100 \cdot e^{-\frac{v}{10}}\ . \tag{6.18}$$

The yaw rate tracking by PI-controller with coefficients $P = 1$ and $I = 3$ is used for the front wheel steering angle. More about yaw rate tracking by PI-controller is described in section [**Yaw-rate tracking**] and diagram for calculation of l_3 distance is shown in [6.3].

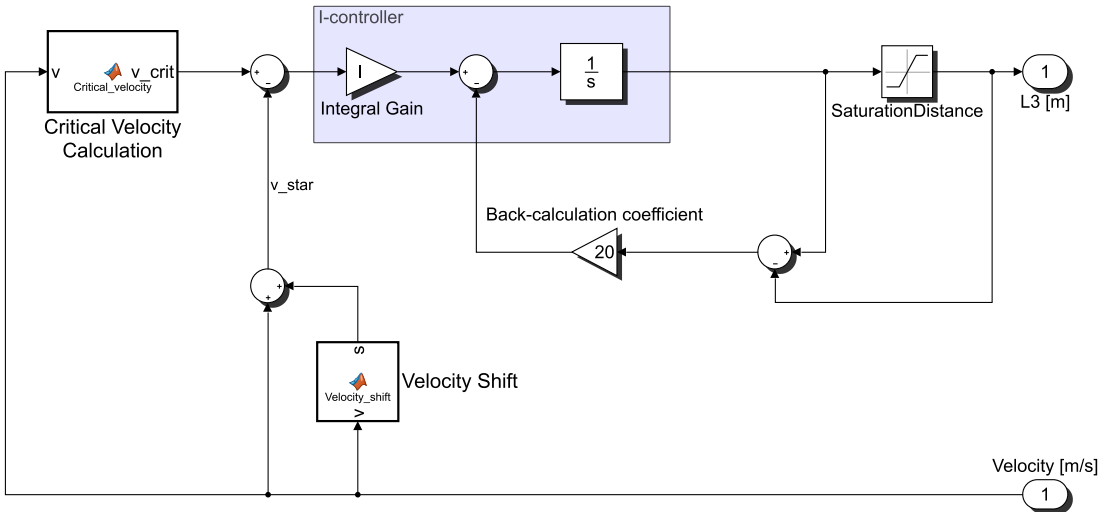

Figure 6.3: Diagram for calculation of l_3 distance with I-controller

7. Influence of Pacejka coefficients on behavior of a vehicle

Most of the vehicles do not have the same Pacejka coefficients for both front and rear wheels. The definition of oversteering and understeering vehicles and their derivation according to the position of CG is evaluated in [10] where it is said that understeering cars have at higher velocities stable complex poles, on the other hand, oversteering cars do not have complex poles and can become unstable. In section [**Parameters**] can be observed, that due to CG in the backside of a vehicle, considered model is an oversteering car. However, it is possible to change oversteering behavior to understeering and vice verse within Pacejka coefficients as well. As an example, the variation of understeering and oversteering behavior dependent on Pacejka coefficient B of parameterized rear wheel with different CG offsets is shown below in figure [7.1], where CG offset is the distance to CG from the middle point of the wheelbase of the car where positive value means shifting to the front and negative to the rear part of the vehicle. The CG offset changes both l_f and l_r. For front wheel all Pacejka coefficients remain the same, meaning D = 1, B = 10, C = 1.45, E = 0.1. For the rear wheel other Pacejka coefficients remain the same as well, meaning D = 1, C = 1.45, E = 0.1. All vehicle parameters stay invariant during this calculation and are taken from section [**Parameters**]. The decision of understeering and oversteering behavior is based on the position of open loop poles.

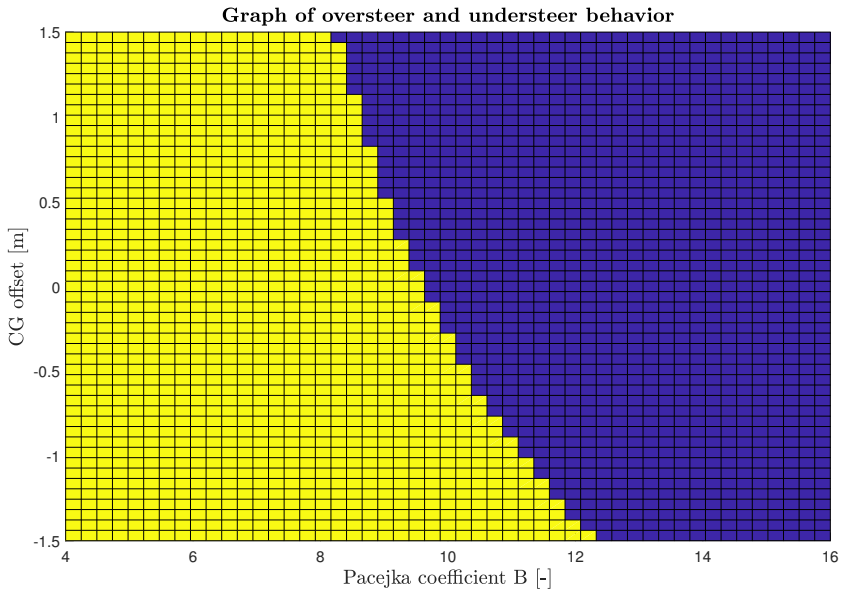

Figure 7.1: Dependency of oversteer (in yellow) and understeer behavior (in blue) on Pacejka coefficient B for lateral force in rear wheel and CG offset

7.1 Change of behavior

In this section, the change of behavior from oversteer to understeer and vice verse is shown.

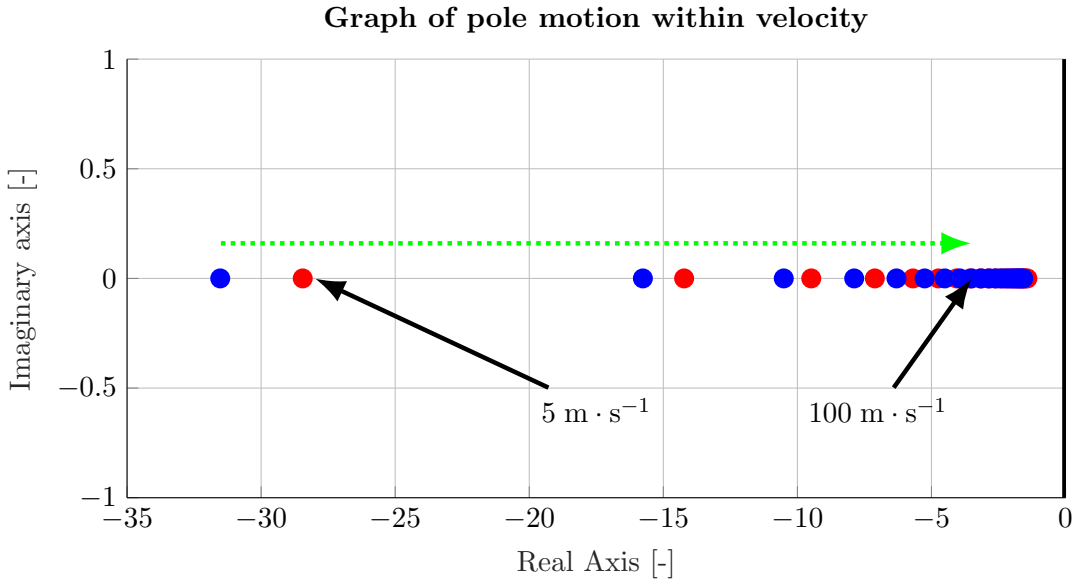

Figure 7.2: Oversteering vehicle with parametres from section [**Parameters**] and same Pacejka coefficients on both wheels as for the front wheels in [4.1], D = 1, C = 1.45, B = 10, E = 0.15.

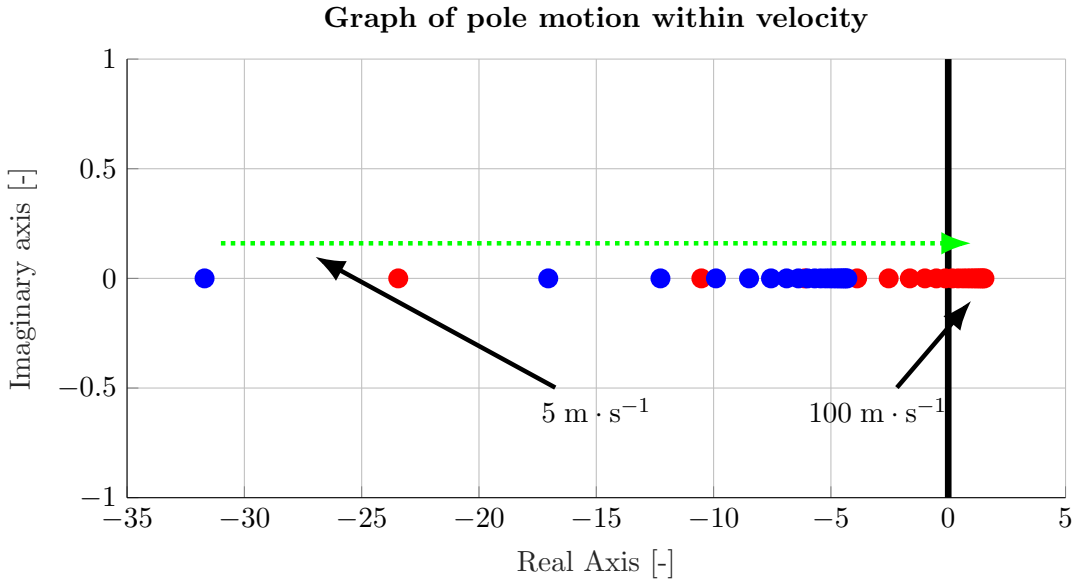

Figure 7.3: Oversteering vehicle shifted to pass stable plane in 44.561 m · s^{-1} from section [**Parameters**] and Pacejka coefficients from [4.1].

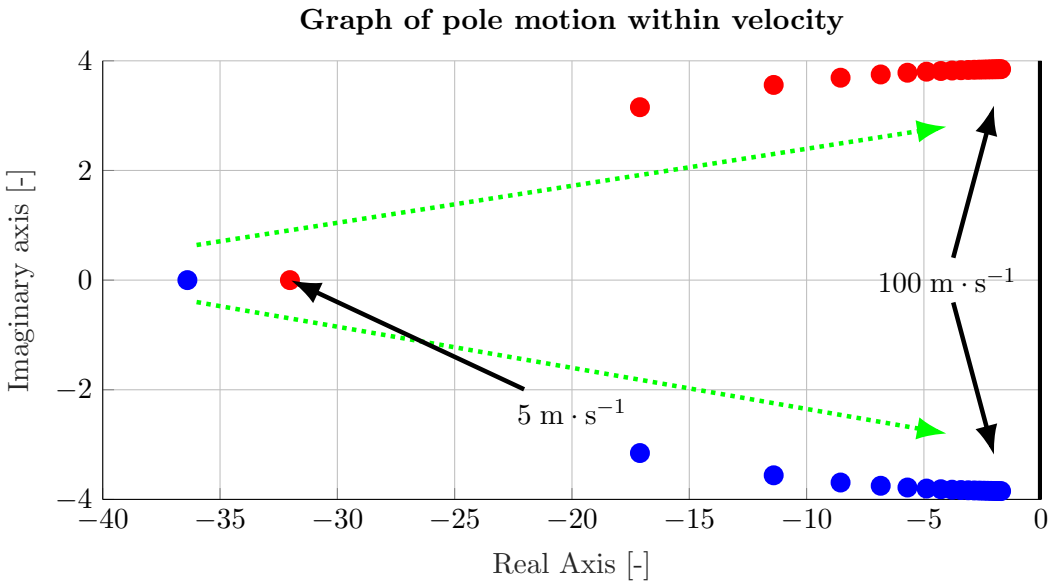

Figure 7.4: Oversteering vehicle transformed to understeering with parametres from section [**Parameters**] and Pacejka coefficients from [4.2].

8. Proposed solutions

8.1 Front tyre slip control

This idea is founded on calculation of the front tyre slip angle α_{fref} straight from wheel input that is regulated by P-controller within feedback of α_f to compute δ_f:

$$\alpha_{fref} = \delta_S - \beta - \frac{l_f}{v} \cdot r \ . \tag{8.1}$$

The rear wheels are used to minimize side-slip angle β as is done in [1]. It is done to stabilize lateral dynamics of the vehicle otherwise the car can get to spin. From equations (4.48) is seen that negative change of value of δ_r have the same effect on $\dot{\beta}$ and opposite on $\dot{r}$. That is why, side slip angle β is assumed to be close to zero for reference calculation of tyre slip angle:

$$\alpha_{fref} = \delta_S - \frac{l_f}{v} \cdot r \ . \tag{8.2}$$

Additionally, α_{fref} is limited to keep tyre slip angle between minimum and maximum peeks seen in [4.5]. Therefore, α_{fref} is saturated on the interval -0.15 rad $< \alpha_{fref} <$ 0.15 rad and so the steering wheel input δ_S needs to be scaled down to accommodate that. It is demonstrated with 'scale' gain in Simulink example [8.3]. Zeros and poles of the system is shown in figures [8.1] below. Transfer function of the understeering behavior of the car is:

$$H(s) = \frac{r(s)}{\delta_S(s)} = 42.989 \cdot \frac{s + 120.4}{(s + 52.02) \cdot (s + 24.79)} \tag{8.3}$$

and of the oversteering behavior of the car:

$$H(s) = \frac{r(s)}{\delta_S(s)} = 42.989 \cdot \frac{s + 78.67}{s^2 + 52.08 \cdot s + 840.7} \ , \tag{8.4}$$

where δ_S is input from the steering wheel and r is yaw rate. Gains of P-constrollers are $P1 = 10$ and $P2 = 10$.

Because of the reason, that it is desirable for the car at higher velocities to follow steering wheel input as much as possible, the PI-controller is used instead of P-controller. New positions of zeros and poles are shown in figures [8.2] below. The transfer function of the understeering behavior of the car changes to following:

$$H(s) = \frac{r(s)}{\delta_S(s)} = 42.989 \cdot \frac{(s + 120.4) \cdot (s + 2.5)}{(s + 52.05) \cdot (s + 24.76) \cdot (s + 2.274)} \tag{8.5}$$

and of the oversteering behavior of the car to:

$$H(s) = \frac{r(s)}{\delta_S(s)} = 42.989 \cdot \frac{(s + 78.67) \cdot (s + 2.5)}{(s + 2.28) \cdot (s^2 + 52.08s + 839.6)} \ , \tag{8.6}$$

where the gains of PI-constroller are $P1 = 10$ and $I = 25$ and P-controller for δ_r is $P2 = 10$. Controller modeled in Simulink is shown below [8.3] where $Lf = l_f$ and $P1$, I and $P2$ are coefficients of mentioned controllers respectively and side slip angle β, yaw rate r, velocity v and front tyre slip angle α_f are inputs from system [**Used modeling approaches**]. Saturations on each wheel are defined in [**Simlutation ride tests**].

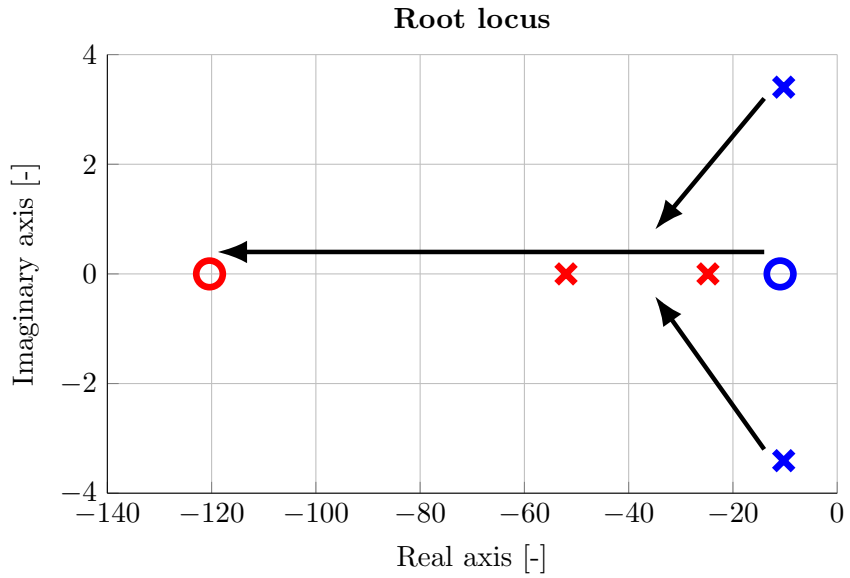

(a) The understeering behavior of the car

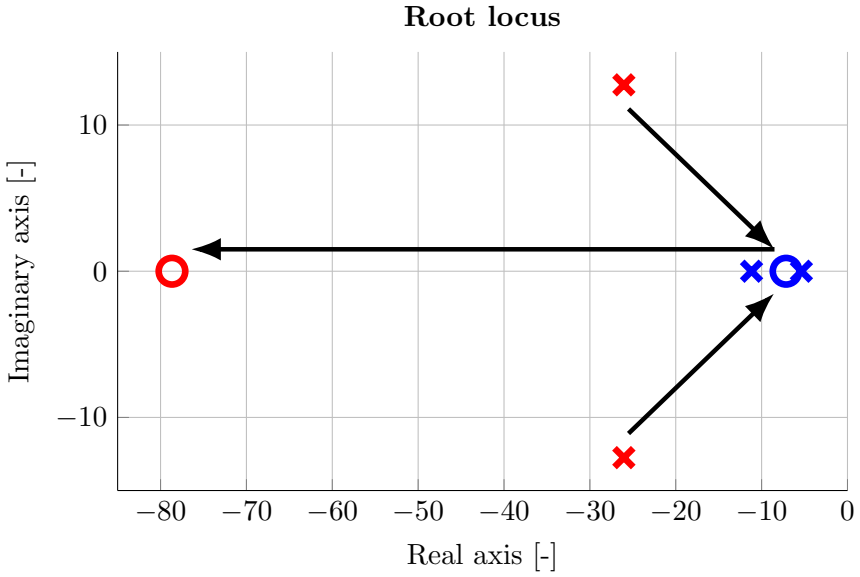

(b) The oversteering behavior of the car

Figure 8.1: Ilustration of shifting of poles and zeros using P-controller of tyre slip angle for $v = 15\ \mathrm{m} \cdot \mathrm{s}^{-1}$ where in red is system with regulator and in blue the base model and arrows from complex poles indicate their movement to the real axis

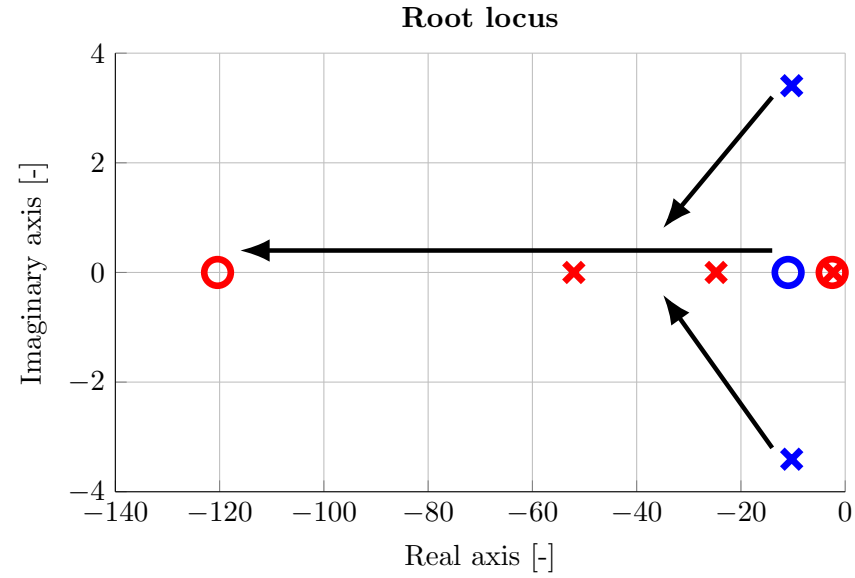

(a) The understeering behavior of the car

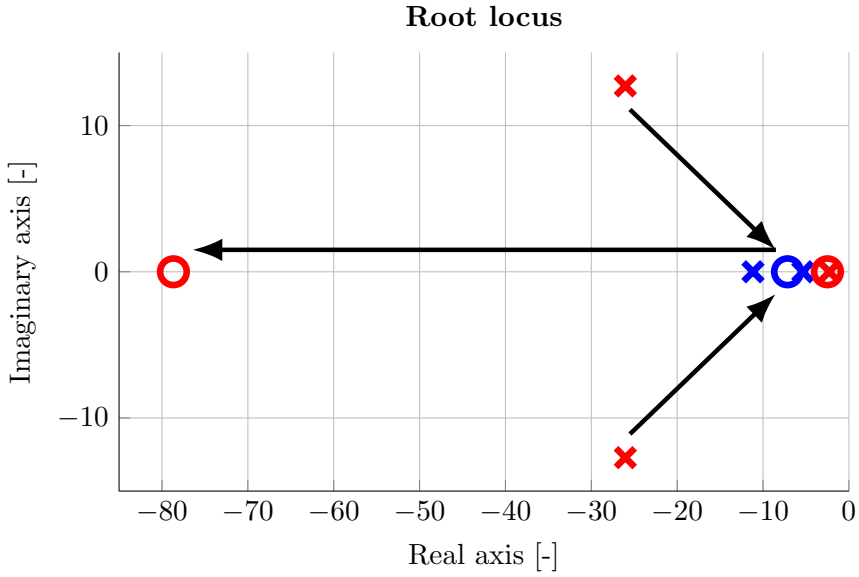

(b) The oversteering behavior of the car

Figure 8.2: Ilustration of shifting of poles and zeros using PI-controller of tyre slip angle for $v = 15\ \mathrm{m} \cdot \mathrm{s}^{-1}$ where in red is system with regulator and in blue the base model and arrows from complex poles indicate their movement to the real axis

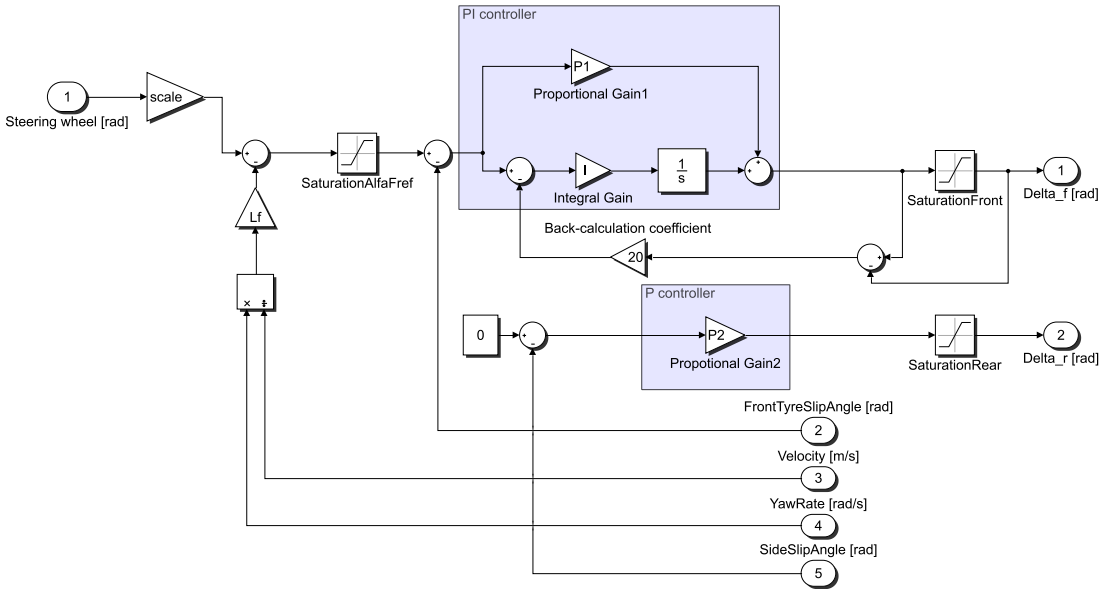

Figure 8.3: Diagram of the front tyre slip PI-controller

8.2 Yaw-rate tracking

The estimation of δ_f is taken from [8]. Used approach for calculating δ_r is regulation around precomputed reference β_r which is the angle between v_{xr} and v_r on the rear wheel. Assuming that $\beta = 0$ then β_r can be defined as:

$$\beta_r = \beta - \frac{l_r}{v} \cdot r = -\frac{l_r}{v} \cdot r \ , \tag{8.7}$$

where r is taken as r_{ref} yaw rate reference. The idea is to control β_r what perfectly damp side slip angle β. The angle δ_r can be then computed from

$$\delta_r = \beta_r + \alpha_r \ , \tag{8.8}$$

but it is not required and in simulations had no effect on maneuverability of the car and so was not used. Zeros and poles of this systems are shown in figures [8.4] below.

The transfer function of the understeering behavior of the car is:

$$H(s) = \frac{r(s)}{r_{ref}(s)} = 138.62 \cdot \frac{(s + 68.49) \cdot (s + 2.434) \cdot (s + 1.12)}{(s + 2.22) \cdot (s + 1.119) \cdot (s^2 + 203.6 \cdot s + 1.042e04)} \ , \tag{8.9}$$

where r_{ref} is reference for yaw rate and r is an output and coefficients of PI-controller for δ_f are $P1 = 2$ and $I = 5$ and PI-controller for δ_r is $P2 = 8$ and $I2 = 10$, and of the oversteering behavior of the car:

$$H(s) = \frac{r(s)}{r_{ref}(s)} = 76.057 \cdot \frac{(s + 38.62) \cdot (s + 10.19) \cdot (s + 1.13)}{(s + 8.929) \cdot (s + 1.129) \cdot (s^2 + 113.8 \cdot s + 3355)} \ , \tag{8.10}$$

where coefficients of PI-controller for δ_f are $P1 = 1$ and $I = 10$ and PI-controller for δ_r is $P2 = 8$ and $I2 = 10$. In picture [8.5], the modeled diagram is shown in

Simulink where side slip angle β, velocity v and yaw rate r are inputs from system [**Used modeling approaches**] and because of the saturations on steering angles the back calculation for prevention of wind-up effect has been employed. Saturations on each wheel are defined in [**Simlutation ride tests**].

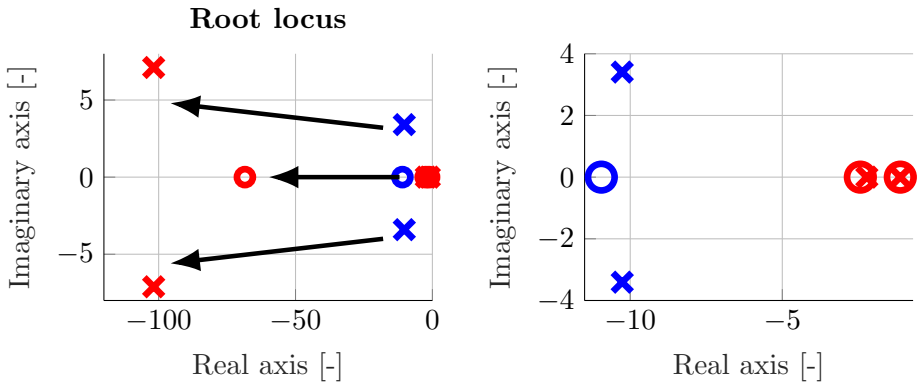

(a) The understeering behavior of the car

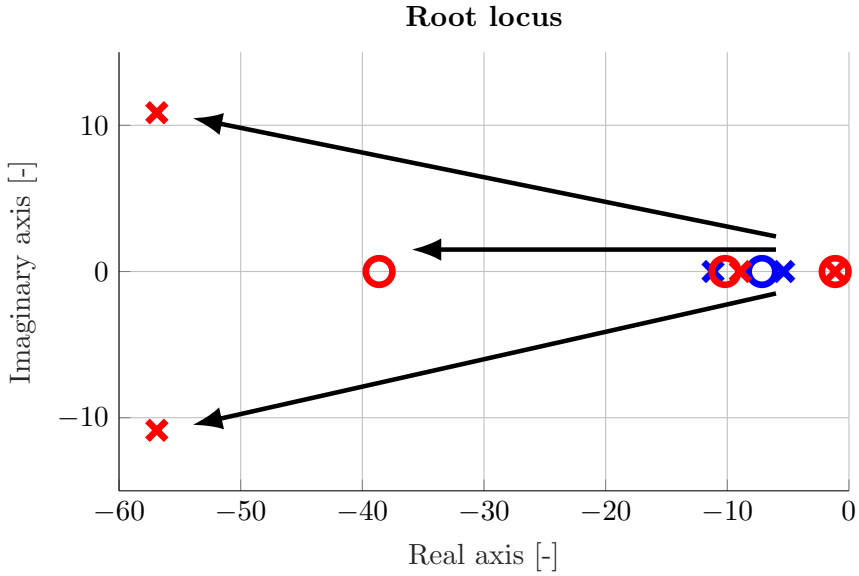

(b) The oversteering behavior of the car

Figure 8.4: Ilustration of shifting of poles and zeros within PI-controller of tyre slip angle for $v = 15\ \mathrm{m} \cdot \mathrm{s}^{-1}$ where in red is system with regulator and in blue the base model and arrows from complex poles indicate their movement to the real axis

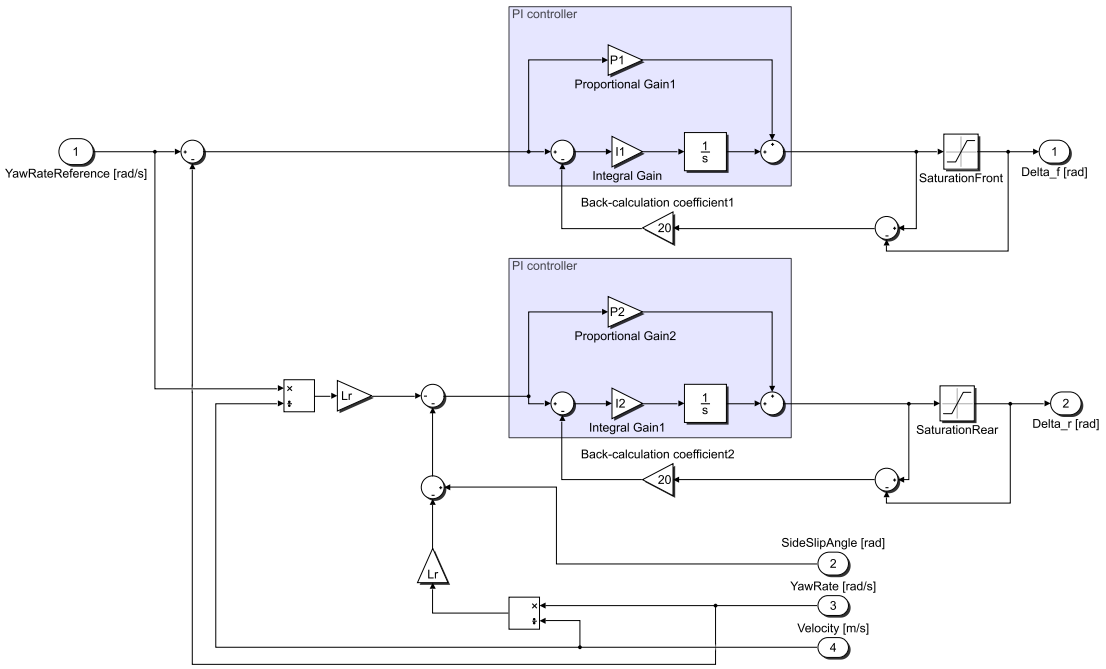

Figure 8.5: Diagram of yaw rate tracking PI-controller where $Lf = l_f$

8.3 Difference of tyre slip angles

This method is based on following equations of tyre slip angles:

$$\alpha_f = \delta_f - \beta - \frac{l_f}{v} \cdot r \ , \tag{8.11}$$

$$\alpha_r = \delta_r - \beta + \frac{l_r}{v} \cdot r \tag{8.12}$$

and taking the difference of (8.11) and (8.12), the following holds

$$\alpha_f - \alpha_r = \delta_f - \delta_r - \frac{l_f + l_r}{v} \cdot r \ . \tag{8.13}$$

Thus, the equation is free of β influence and with assumption $\alpha_f - \alpha_r = 0$ also relation between steer angles δ_f, δ_r and yaw rate r has been derived. With simple algebraitic steps applies following formula

$$\delta_f = \delta_r + \frac{l_f + l_r}{v} \cdot r \ , \tag{8.14}$$

where yaw rate r can be taken as reference r_{ref} and so the definition of δ_f is derived. Nevertheless, a given system has big deviation of referenced input and so there was added PI-controller to r_{ref}

$$\delta_f = \delta_r + \frac{l}{v} \cdot r_{ref} \ , \tag{8.15}$$

where $l = l_f + l_r$. The steer angle δ_r is computed with P-controller that minizes side slip angle β. Shifting of poles and zeros is shown in figures [8.4] below.

The transfer function of the understeering behavior of the car is:

$$H(s) = \frac{r(s)}{r_{ref}(s)} = 136.61 \cdot \frac{(s + 36.49) \cdot (s + 2.769)}{(s + 140.9) \cdot (s + 37.82) \cdot (s + 2.591)} \tag{8.16}$$

and of the oversteering behavior of the car:

$$H(s) = \frac{r(s)}{r_{ref}(s)} = 136.61 \cdot \frac{(s + 23.84) \cdot (s + 2.769)}{(s + 146.3) \cdot (s + 23.31) \cdot (s + 2.644)} , \tag{8.17}$$

where r_{ref} is referenced for yaw rate and r is an output and coefficients of PI-controller are $P1 = 13$ and $I = 36$ and P-controller for δ_r is $P2 = 2$. In picture [8.7], the controller diagram in Simulink is shown where side slip angle β and yaw rate r are inputs from system in chapter [**Used modeling approaches**], $L = l_f + l_r$ and because of saturations on steering angles there is a back calculation preventing wind-up effect. Saturations on each wheel are defined in [**Simlutation ride tests**].

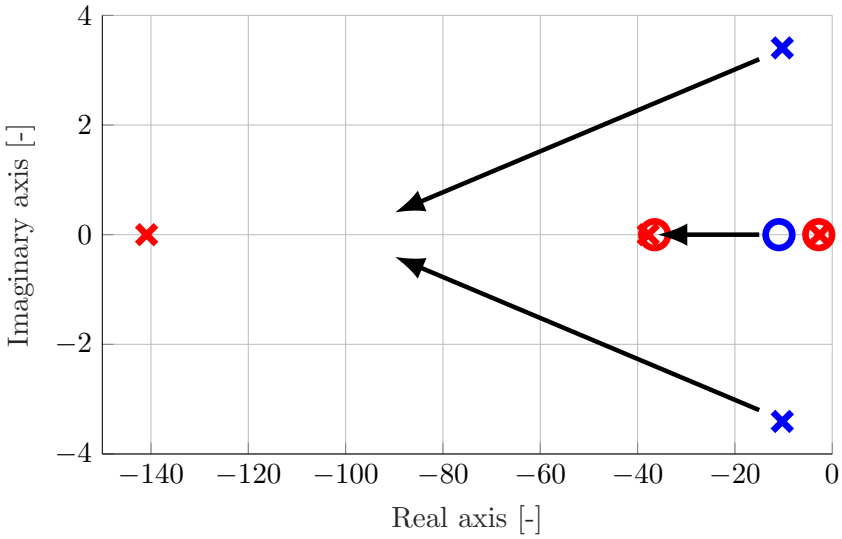

(a) The understeering behavior of the car

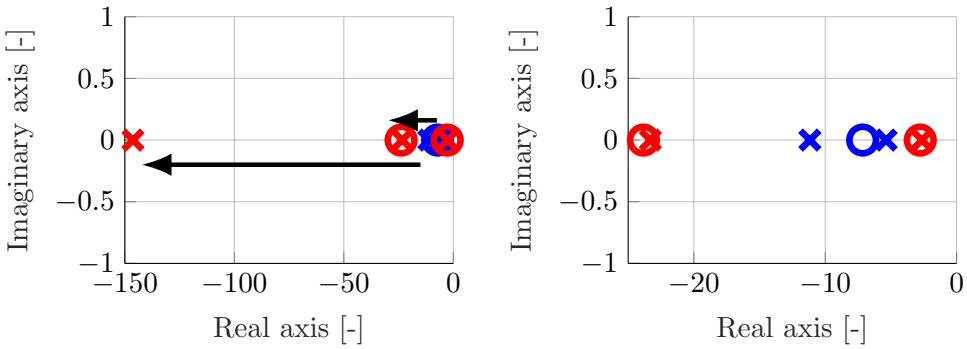

(b) The oversteering behavior of the car

Figure 8.6: Ilustration of shifting of poles and zeros within PI-controller of tyre slip angle for $v = 15\ \mathrm{m} \cdot \mathrm{s}^{-1}$ where in red is system with regulator and in blue the base model and arrows from complex poles indicate their movement to the real axis

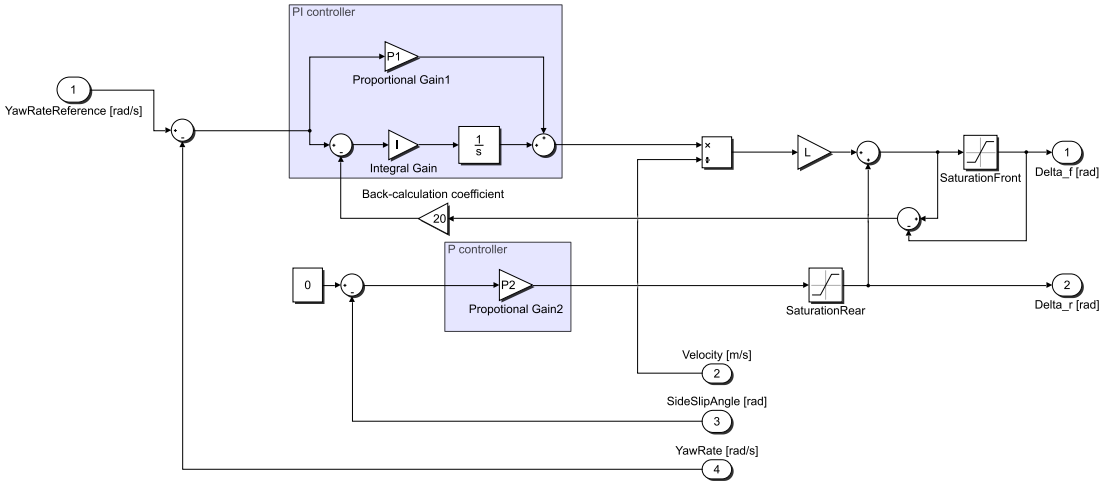

Figure 8.7: Diagram of calculating steering angles with equation (8.15) PI-controller

9. Simlutation ride tests

The controllers proposed in chapter [**Proposed solutions**] are derived on single-track model described in chapter [**Used modeling approaches**]. However, their testing will be carried out on twin-track model, succesfully comparing their usability and functionality on more realistic and high-fidelity models. The test will reference double lane change maneuver as steering wheel input from the driver shown in graph [9.1] for velocity $v = 15\ \mathrm{m \cdot s^{-1}}$ and $v = 35\ \mathrm{m \cdot s^{-1}}$ and will have two parts. Firstly, as an example of the effect of an enviroment, the reaction on wind blowing to the side of the car is tested. For instance, the real life example can be invisioned by a car on a highway entering an open area like a bridge. It is realized by sinus-like step-change in side slip angle β for 0.2 rad shown below in [9.2]. Secondly, change of friction between surface of road for wheels on right side of the vehicle will be realized via changing of Pacejka coefficient D by step-change to 0.4, implementing an entry on grass-rock surface. Only graphs demonstrating reference following and steer angles inputs will be shown. Lastly, the wheels in vehicle's chassis are limited by maximal angle to which they can rotate to and that was modeled by saturation blocks from $-\frac{\pi}{6} < \delta_i < \frac{\pi}{6}$ for both steering angles. This causes nonlinear behavior and results in wind-up. Used solution of anti-wind up is back calculation algorithm.

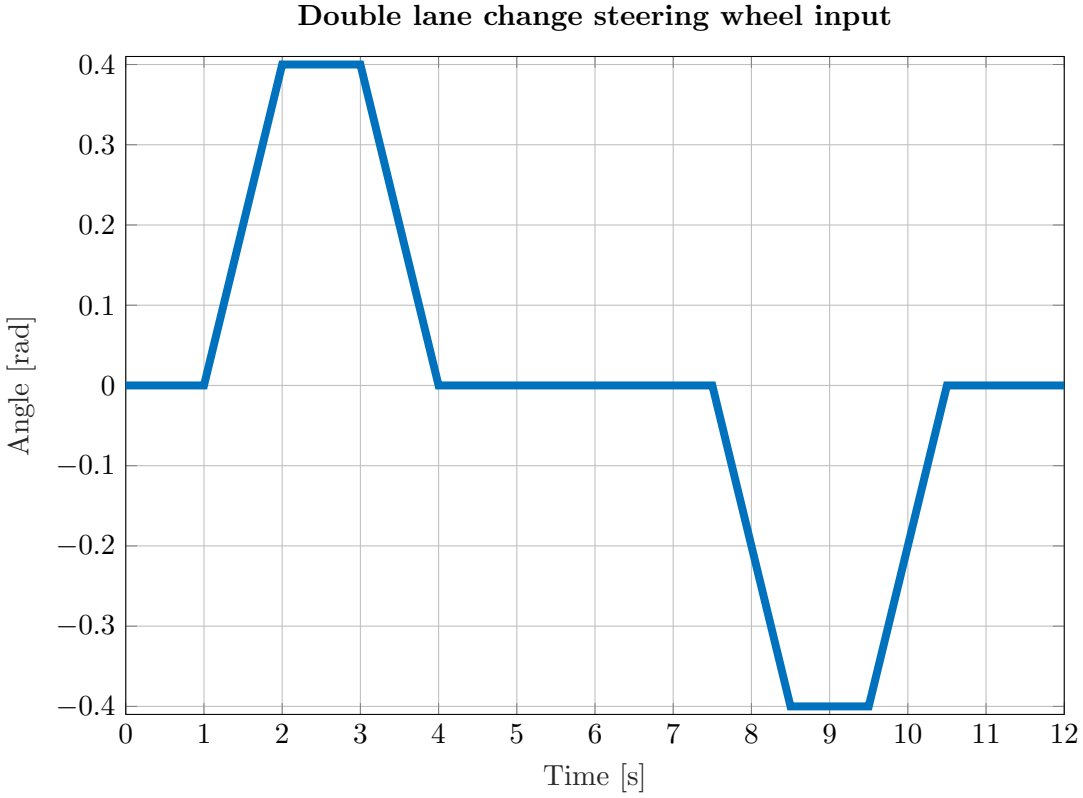

Figure 9.1: Steering wheel input δ_S for double lane change maneuver

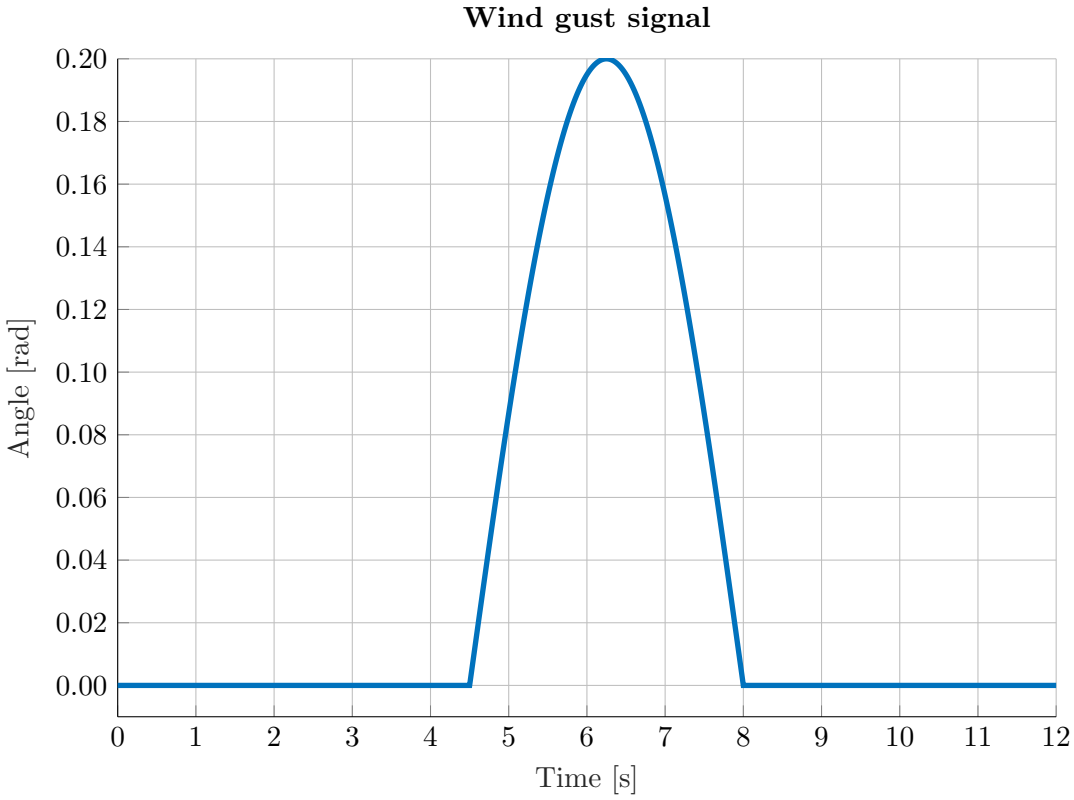

Figure 9.2: Step change of side slip angle β for double lane change maneuver

9.1 Input conversions

Because each of proposed controllers do not have the same input variable, the nessesary conversion was derived as in [1] like

$$a_{fref}(t) = k_f(v) \cdot \delta_S(t) = \frac{l \cdot c_f \cdot c_r \cdot v(t)^2}{c_f \cdot c_r \cdot l^2 + m \cdot v(t)^2 \cdot (c_r \cdot l_r - c_f \cdot l_f)} \cdot \delta_S(t) \ , \tag{9.1}$$

where $a_{fref}(t)$ is referenced lateral acceleration of the front axle, $\delta_S(t)$ steering wheel input, c_f and c_r front and rear cornering stiffness coefficients respectively, m mass of the vehicle and $l = l_f + l_r$ where l_f and l_r are distance from CG to front and rear axle respectively.

Next, the reference for yaw rate r_{ref} can be derived in stationary cornering along a circular path with radius R and it's centripetal acceleration a_f. The yaw rate equals $r = v/R$ with $a_f = v^2/R$ and so conversion is

$$r_{ref}(t) = \frac{a_{fref}(t)}{v(t)} = \frac{l \cdot c_f \cdot c_r \cdot v(t)}{c_f \cdot c_r \cdot l^2 + m \cdot v(t)^2 \cdot (c_r \cdot l_r - c_f \cdot l_f)} \cdot \delta_S(t) \ . \tag{9.2}$$

The member $(c_r \cdot l_r - c_f \cdot l_f)$ equals almost zero when the same Pacejka coefficients are used for both front and rear wheel, making $r_{ref}(t) = v(t)/l$ and gain $k_f(v)$ too large, and so different coefficients were used effectively making vehicle more realistic. However, the gain $k_f(v)$ is getting higher with higher velocity, making lateral acceleration in

hundreds when steering wheel input around 30^o degrees and velocity 30 $\mathrm{m} \cdot \mathrm{s}^{-1}$. One solution is to divide δ_S by steering gear ration N as derived in [4] but there are no definitions of how exactly is the value of N changed between different velocities. That is why, reference was calculated differently.

First, yaw rate r was recorded with maximal steering wheel input 35^o during different velocities and with formula

$$R = \frac{v}{r} \tag{9.3}$$

was turning radius calculated and it's dependence on velocity v approximated as quadratic function for the understeering behavior of used car:

$$R = 0.1367 \cdot \mathrm{v}^2 - 0.3450 \cdot \mathrm{v} + 2.5719 \tag{9.4}$$

and of used oversteering car:

$$R = 0.1430 \cdot \mathrm{v}^2 - 0.2334 \cdot \mathrm{v} + 2.3140 \ . \tag{9.5}$$

With that, reference for yaw rate r_{ref} is calculated and scaled by steering wheel input δ_S as:

$$r = \frac{v}{R} \cdot \delta_S^* \ , \tag{9.6}$$

where δ_S^* is δ_S divided by maximal steering wheel input. Then, the front lateral acceleration of the front axle a_f can by computed by

$$a_f = r \cdot v \tag{9.7}$$

as derived in [1].

9.2 Parameters

Here, all the coeffiecients and parametres of test vehicle are listed.

Symbol	Value	Describtion
m	1190 kg	mass of vehicle
l_f	1.6387 m	distance between CG and front axle
l_r	1.3613 m	distance between CG and rear axle
c_f^u	76812 $\mathrm{N \cdot rad^{-1}}$	front cornering stiffness coefficient for the understeering behavior
c_r^u	118603 $\mathrm{N \cdot rad^{-1}}$	rear cornering stiffness coefficient for the understeering behavior
c_f^o	76812 $\mathrm{N \cdot rad^{-1}}$	front cornering stiffness coefficient for the oversteering behavior
c_r^o	77474 $\mathrm{N \cdot rad^{-1}}$	rear cornering stiffness coefficient for the oversteering behavior
F_{zf}	5297 N	front wheel load force
F_{zr}	6377 N	rear wheel load force
v	15 $\mathrm{m \cdot s^{-1}}$	velocity (not in simulator)
R_f	0.33 m	front wheel radius
R_r	0.33 m	rear wheel radius
J_f	1 $\mathrm{kg \cdot m^2}$	moment of inertia along y-axis of front wheel
J_r	1 $\mathrm{kg \cdot m^2}$	moment of inertia along y-axis of rear wheel
J	2396 $\mathrm{kg \cdot m^2}$	moment of inertia along z-axis of CG
k_f	2 $\mathrm{N \cdot s}$	front coefficient of road drag
k_r	2 $\mathrm{N \cdot s}$	rear coefficient of road drag
T	140 $\mathrm{deg \cdot s^{-1}}$	slew rate of steering angles

Table 9.1: Parametres and coefficients used in test vehicle

The Pacejka Magic Formula coefficients are listed in chapter [**Robust decoupling**] in [4.2] and [4.1]. The cornering stiffness coefficients were calculated from equation $c_i = B \cdot C \cdot D \cdot F_{zi}$ that is approximation of derivation of formula $c_i = \frac{\mathrm{d}F_{yi}}{\mathrm{d}\alpha_i}$ in zero where i stands for front and rear and B, C, D are Pacejka coefficients from [4.2] and [4.1]. Because of the position of center of gravity on the backside, the vehicle tends to oversteer, meaning that car curves more than neutral steering car during cornering and can become unstable when critical velocity is reached. However, this tendency can be changed by different Pacejka coefficients as was mentioned in [**Influence of Pacejka coefficients on behavior of a vehicle**]. As can be observed in table [9.1], testing vehicle is a sport car.

9.3 Front tyre slip control test

The referenced steering wheel input in [9.1] is scaled by proportional gain to have maximum of 0.1 rad. This controller does not follow yaw rate reference because it's feedback loop is on front tyre slip angle α_f. Hovewer, the graphs will be shown for

comparison and influence of deviations on it. The coefficients for PI-controller are from [**Front tyre slip control**]. The start of deviations is indicated by black dashed line:

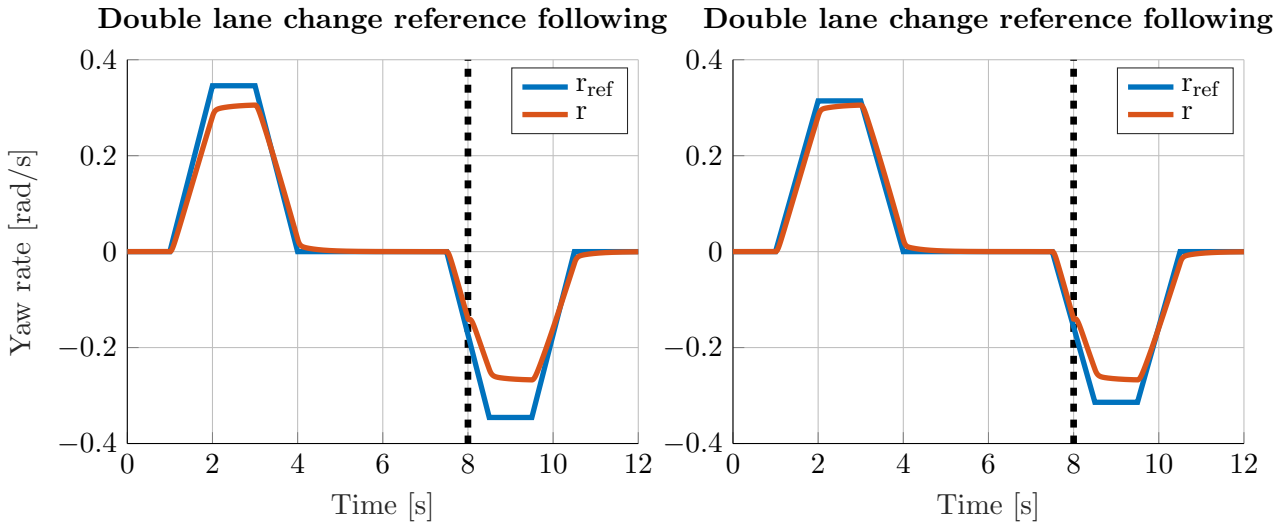

(a) The understeering behavior of the car (b) The oversteering behavior of the car

Figure 9.3: Front tyre slip control reference following for double lane change maneuver for $v = 15\ \mathrm{m} \cdot \mathrm{s}^{-1}$ where Pacejka coefficient D of rightside wheels is set to 0.4 in 8 s.

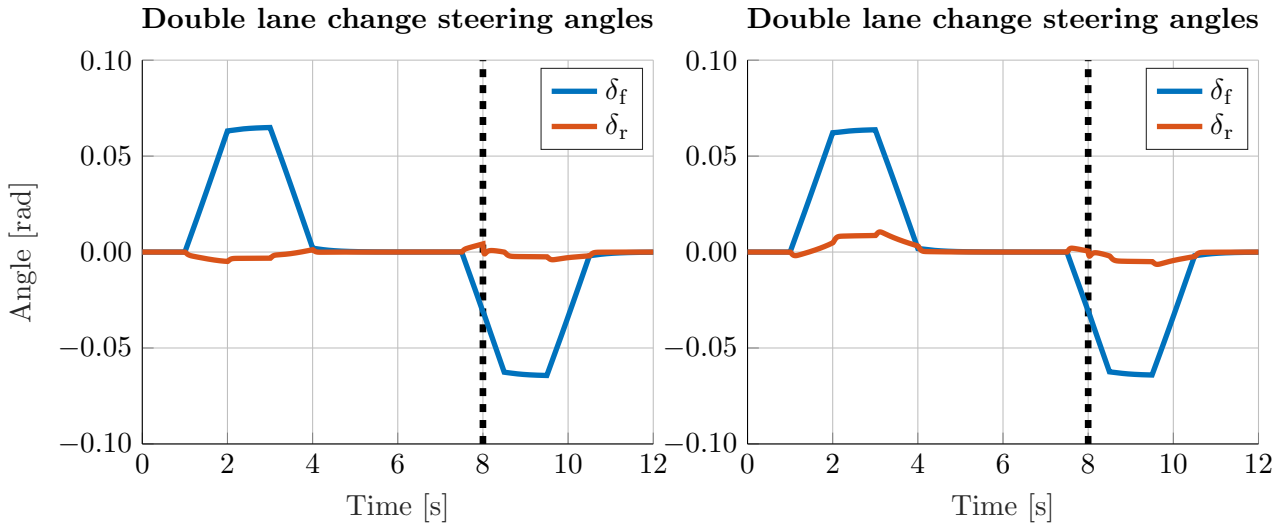

(a) The understeering behavior of the car (b) The oversteering behavior of the car

Figure 9.4: Front tyre slip control reference following for double lane change maneuver for $v = 15\ \mathrm{m} \cdot \mathrm{s}^{-1}$ where Pacejka coefficient D of rightside wheels is set to 0.4 in 8 s.

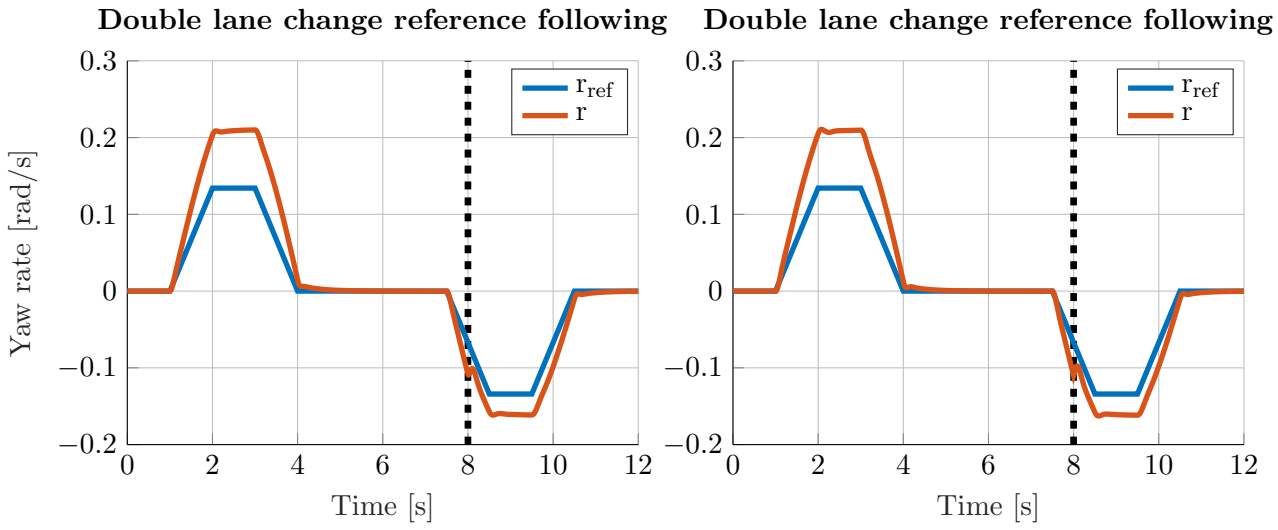

(a) The understeering behavior of the car (b) The oversteering behavior of the car

Figure 9.5: Front tyre slip control reference following for double lane change maneuver for $v = 35\ \mathrm{m} \cdot \mathrm{s}^{-1}$ where Pacejka coefficient D of rightside wheels is set to 0.4 in 8 s.

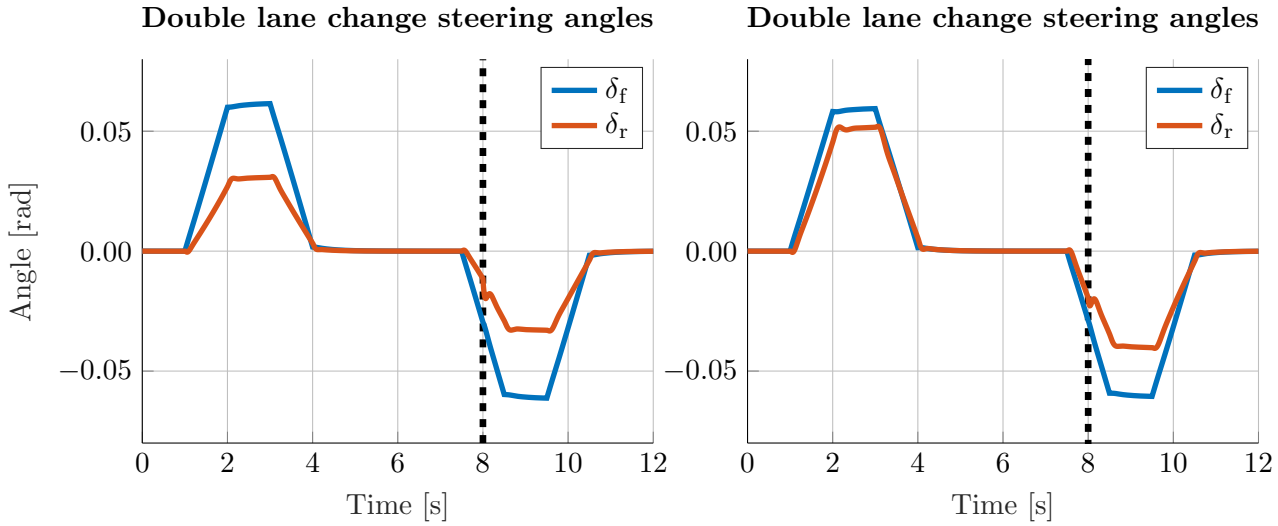

(a) The understeering behavior of the car (b) The oversteering behavior of the car

Figure 9.6: Front tyre slip control reference following for double lane change maneuver for $v = 35\ \mathrm{m} \cdot \mathrm{s}^{-1}$ where Pacejka coefficient D of rightside wheels is set to 0.4 in 8 s.

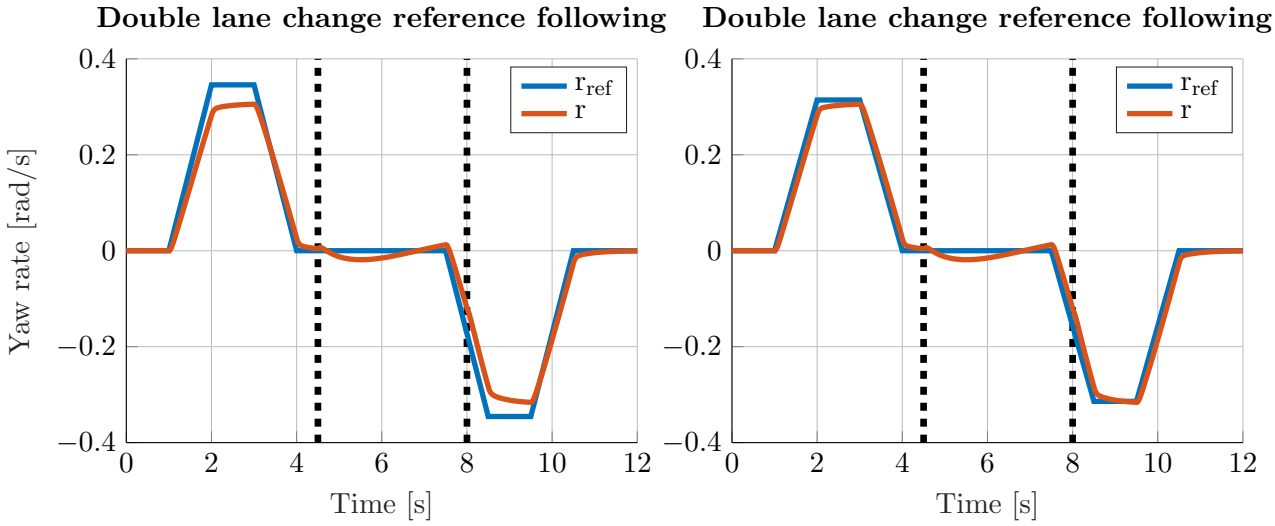

(a) The understeering behavior of the car (b) The oversteering behavior of the car

Figure 9.7: Front tyre slip control reference following for double lane change maneuver for $v = 15\ \mathrm{m} \cdot \mathrm{s}^{-1}$ for step-change of β as in [9.2].

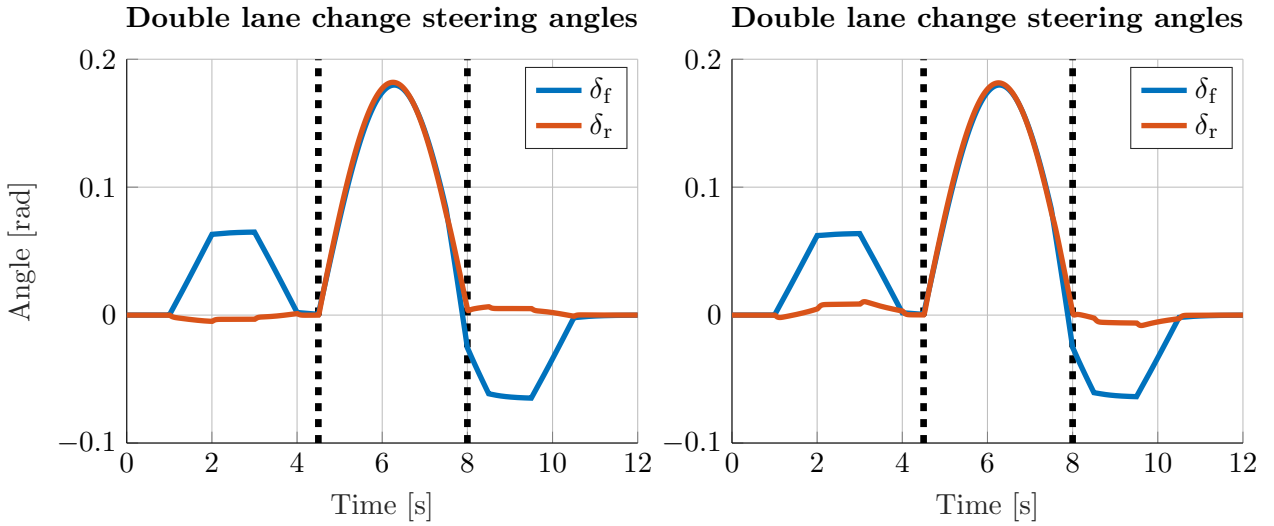

(a) The understeering behavior of the car (b) The oversteering behavior of the car

Figure 9.8: Front tyre slip control reference following for double lane change maneuver for $v = 15\ \mathrm{m} \cdot \mathrm{s}^{-1}$ for step-change of β as in [9.2].

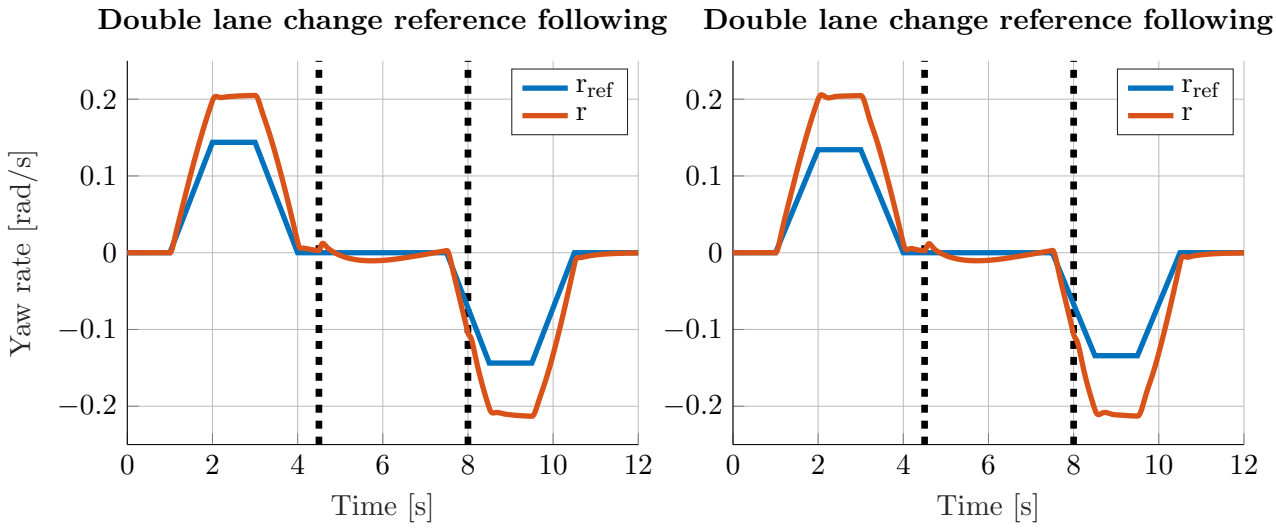

(a) The understeering behavior of the car (b) The oversteering behavior of the car

Figure 9.9: Front tyre slip control reference following for double lane change maneuver for $v = 35\ \mathrm{m} \cdot \mathrm{s}^{-1}$ for step-change of β as in [9.2].

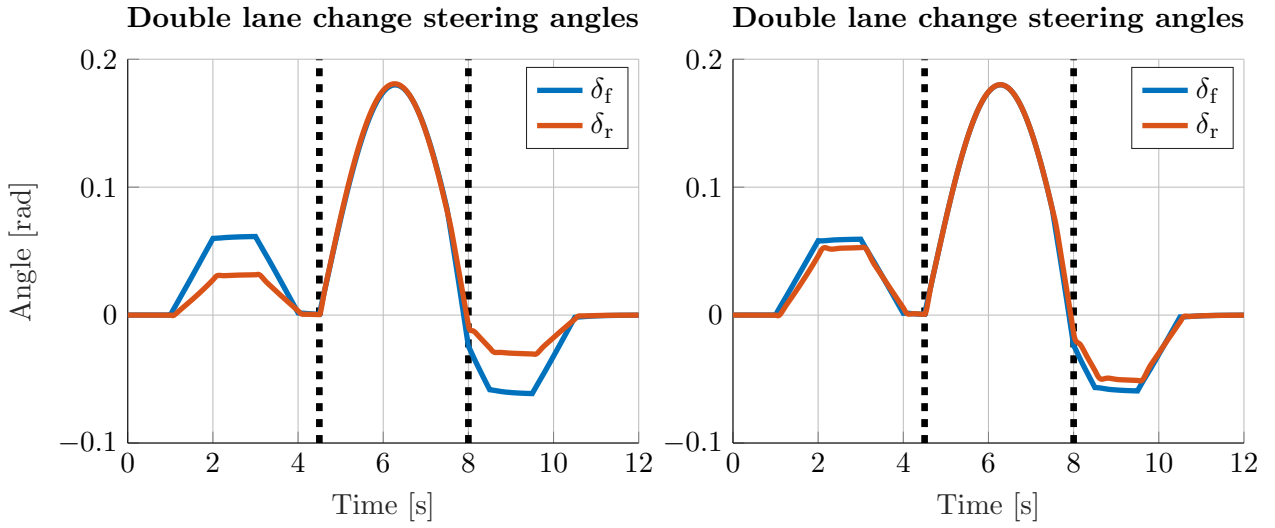

(a) The understeering behavior of the car (b) The oversteering behavior of the car

Figure 9.10: Front tyre slip control reference following for double lane change maneuver for $v = 35\ \mathrm{m} \cdot \mathrm{s}^{-1}$ for step-change of β as in [9.2].

From figures [9.3] and [9.4] can be observed that change of terrain on right vehicle wheels does lower yaw rate r because the steering is following δ_{fref} reference. Next, steering angle δ_r is changing sign for the understeering behavior of the car according to speed of the vehicle which is desired because in higher velocities are even sign for δ_f and δ_r better for double lane change maneuvers and for lower velocities different for sharper cornering. Step-change of side slip angle β has little effect on behavior of car besides produced backspike in yaw rate r in [9.9] which is expected. Moreover, car is capable of sharper turns than with yaw rate reference r_{ref} due to direct control from δ_S which can be seen in [9.9]. However, testing has shown that car is still not completely

stable and can get to spin. Mainly during sharp cornering with high acceleration and so more testing and changes are needed.

9.4 Yaw-rate tracking test

The referenced steering wheel input in [9.1] is converted to yaw rate r_{ref} by [**Input conversions**] with equation [9.6] and is followed with PI-controller with coefficients from [**Yaw-rate tracking**]. The start of deviations is indicated by black dashed line:

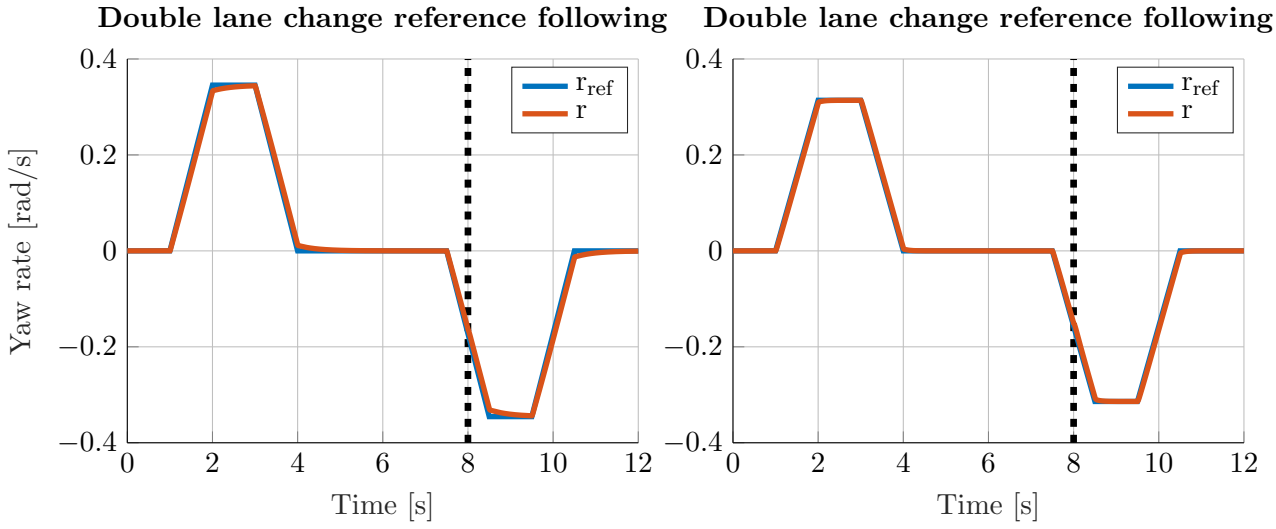

(a) The understeering behavior of the car (b) The oversteering behavior of the car

Figure 9.11: Yaw rate tracking reference following for double lane change maneuver for $v = 15\ \mathrm{m} \cdot \mathrm{s}^{-1}$ for step-change of Pacejka coefficient D of rightside wheels to 0.4 in 8 s.

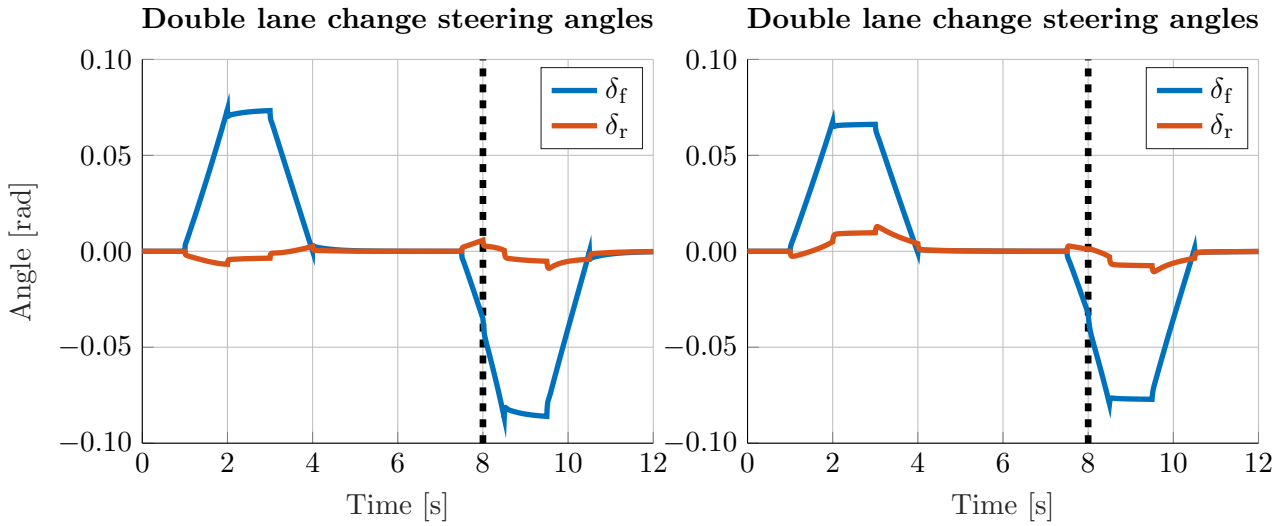

(a) The understeering behavior of the car (b) The oversteering behavior of the car

Figure 9.12: Yaw rate tracking steer angle inputs for double lane change maneuver for $v = 15\ \mathrm{m} \cdot \mathrm{s}^{-1}$ for step-change of Pacejka coefficient D of rightside wheels to 0.4 in 8 s.

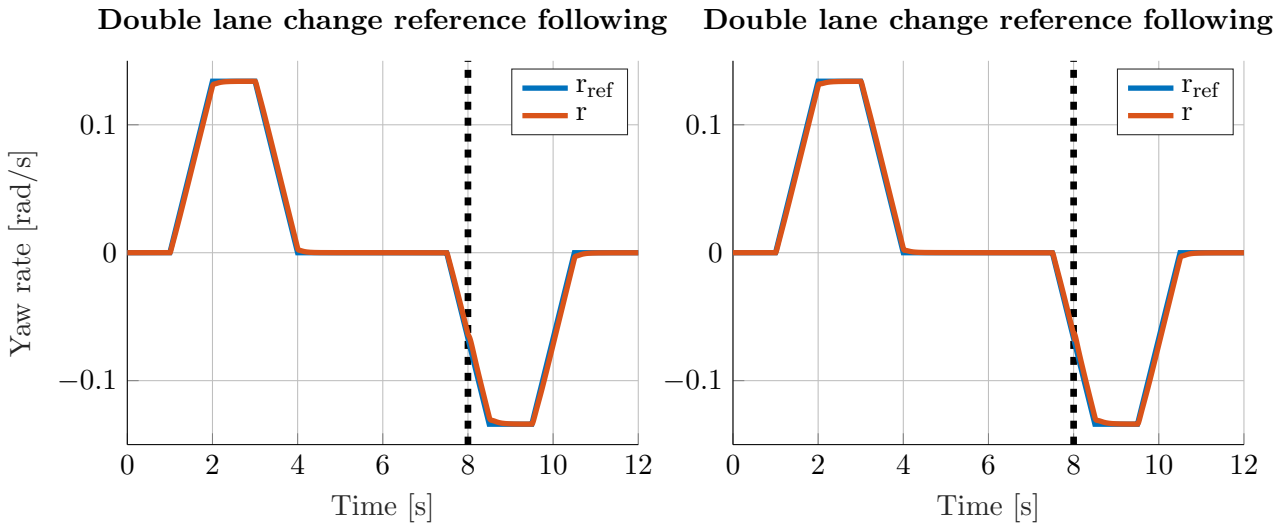

(a) The understeering behavior of the car (b) The oversteering behavior of the car

Figure 9.13: Yaw rate tracking reference following for double lane change maneuver for $v = 35\ \mathrm{m} \cdot \mathrm{s}^{-1}$ for step-change of Pacejka coefficient D of rightside wheels to 0.4 in 8 s.

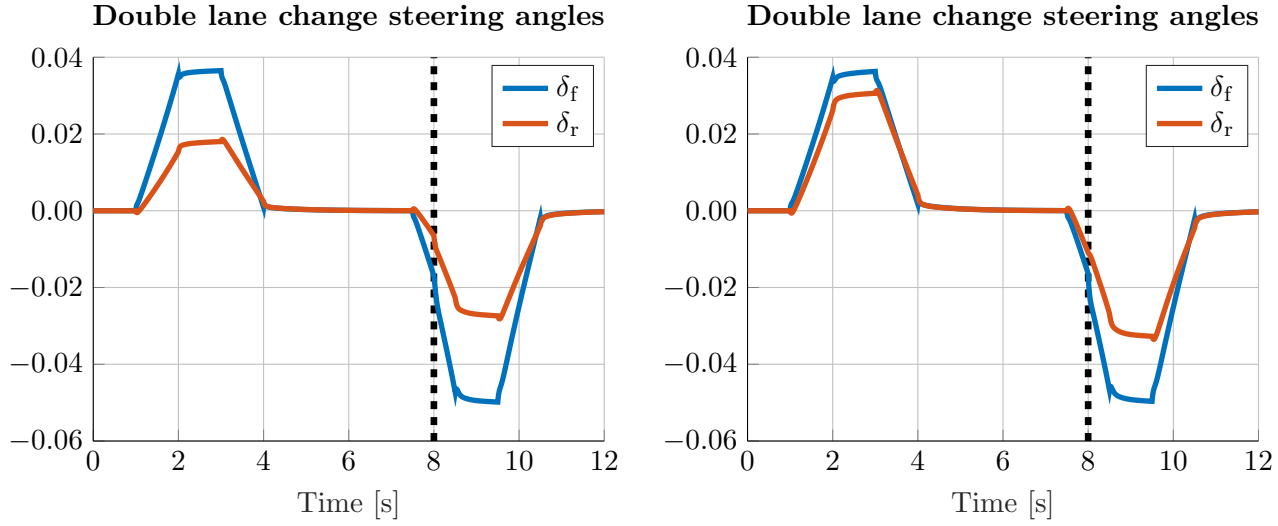

(a) The understeering behavior of the car (b) The oversteering behavior of the car

Figure 9.14: Yaw rate tracking steer angle inputs for double lane change maneuver for $v = 35\ \mathrm{m} \cdot \mathrm{s}^{-1}$ for step-change of Pacejka coefficient D of rightside wheels to 0.4 in 8 s.

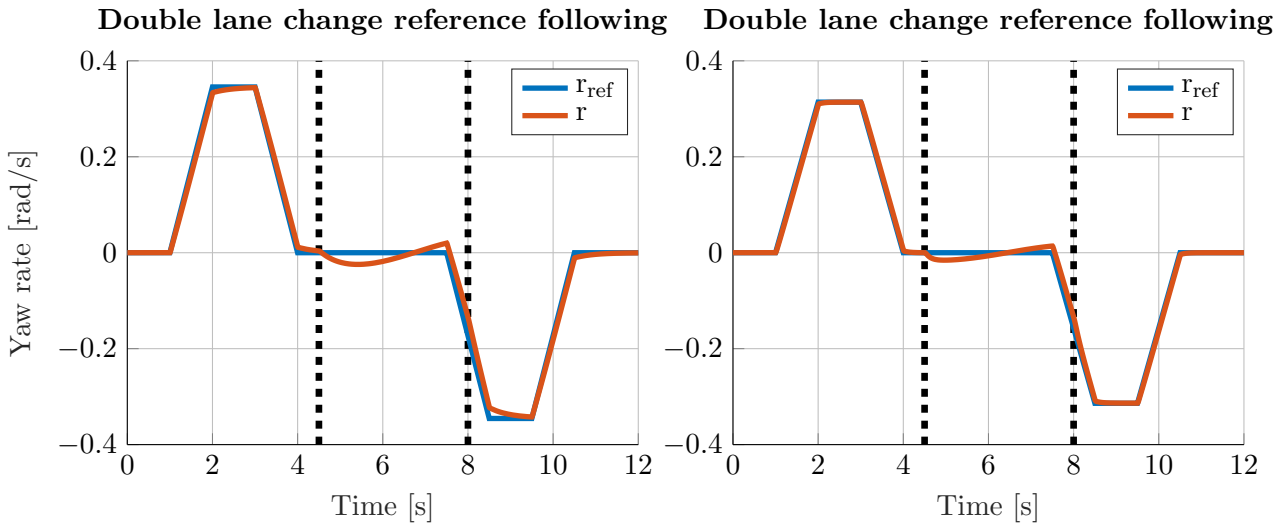

(a) The understeering behavior of the car (b) The oversteering behavior of the car

Figure 9.15: Yaw rate tracking reference following for double lane change maneuver for $v = 15\ \mathrm{m} \cdot \mathrm{s}^{-1}$ for step-change of β as in [9.2].

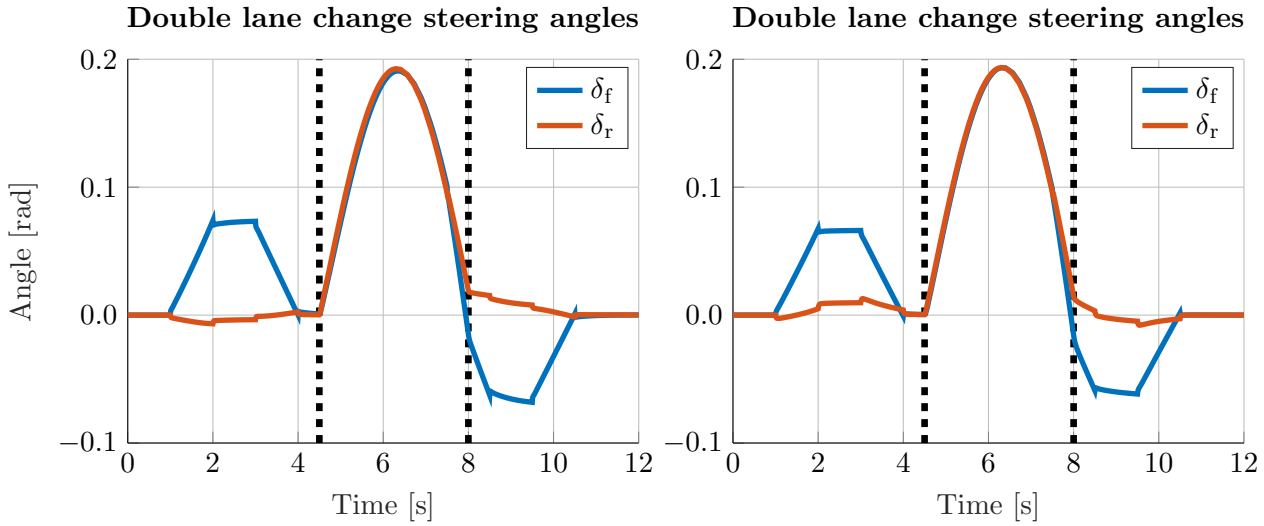

(a) The understeering behavior of the car (b) The oversteering behavior of the car

Figure 9.16: Yaw rate tracking steer angle inputs for double lane change maneuver for $v = 15\ \mathrm{m} \cdot \mathrm{s}^{-1}$ for step-change of β as in [9.2].

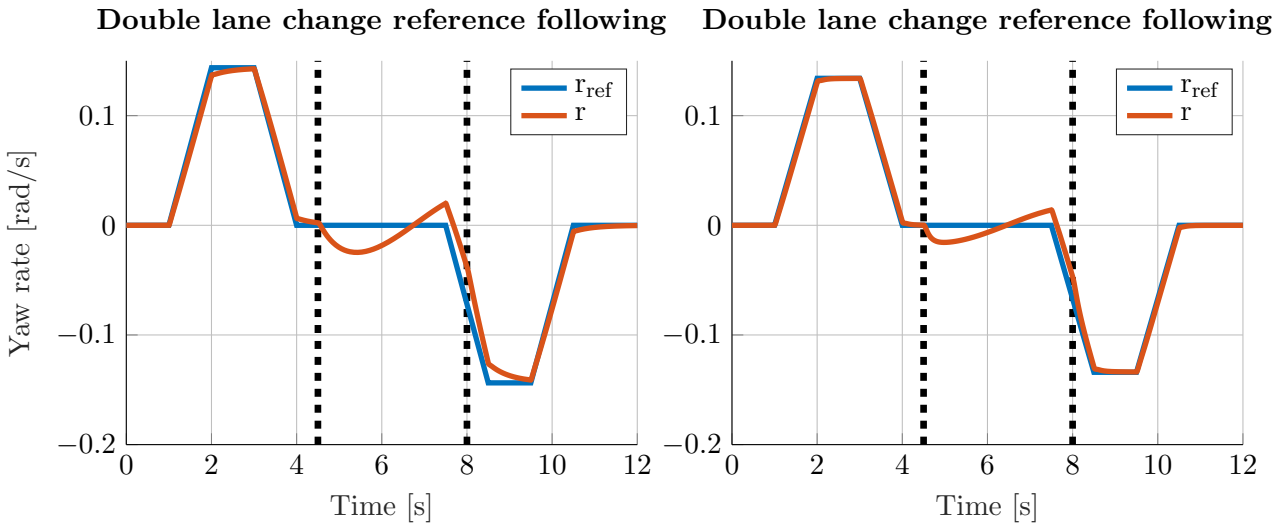

(a) The understeering behavior of the car (b) The oversteering behavior of the car

Figure 9.17: Yaw rate tracking reference following for double lane change maneuver for $v = 35\ \mathrm{m} \cdot \mathrm{s}^{-1}$ for step-change of β as in [9.2].

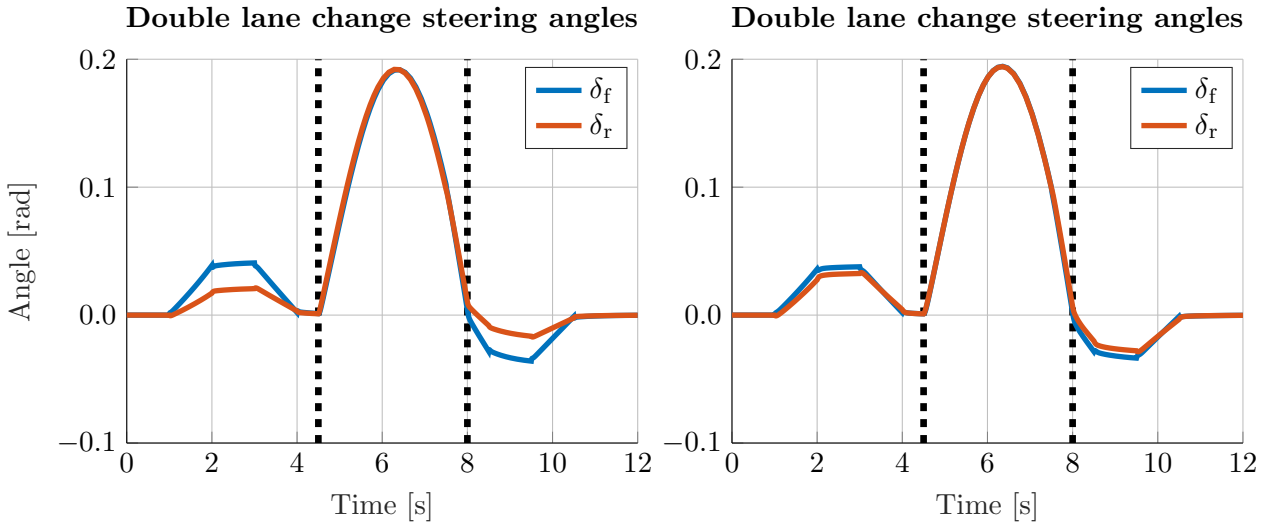

(a) The understeering behavior of the car (b) The oversteering behavior of the car

Figure 9.18: Yaw rate tracking steer angle inputs for double lane change maneuver for $v = 35\ \mathrm{m} \cdot \mathrm{s}^{-1}$ for step-change of β as in [9.2].

From figures [9.11] and [9.16] can be evalueted that entry of right vehicles wheels on grass-rock surface has low or zero effect on regulation. Next, steering angle δ_r is changing sign according to speed of vehicle aswel. The problem can be seen in [9.15] and [9.17] where due to step-change of side slip angle β is produced spike which is getting bigger with higher velocity. The β_r steering allows rear wheels on low velocities to control spin in a such a way that they steer into manuever rather than be perpendicularly to it and so car is capable of turning very easily.

9.5 Difference of tyre slip angles test

The referenced steering wheel input in [9.1] is converted to yaw rate r_{ref} by [**Input conversions**] using equation [9.6] and is followed with PI-controller with coefficients from [**Difference of tyre slip angles**]. The start of deviations is indicated by black dashed line:

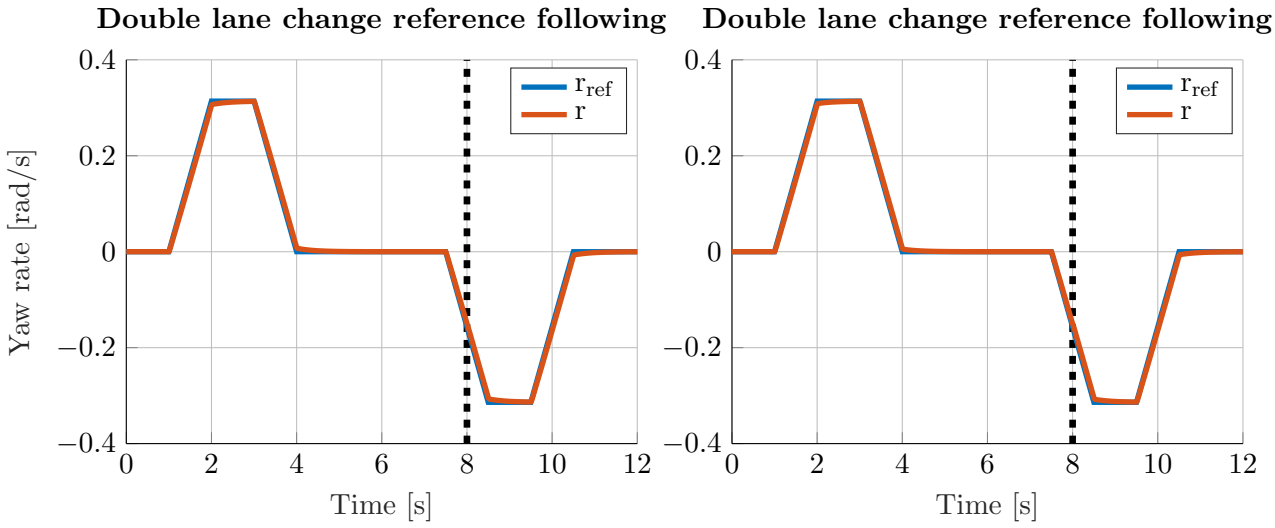

(a) The understeering behavior of the car (b) The oversteering behavior of the car

Figure 9.19: Difference α_i control reference following for double lane change maneuver for $v = 15\ \mathrm{m \cdot s^{-1}}$ where Pacejka coefficient D of rightside wheels is set to 0.4 in 8 s.

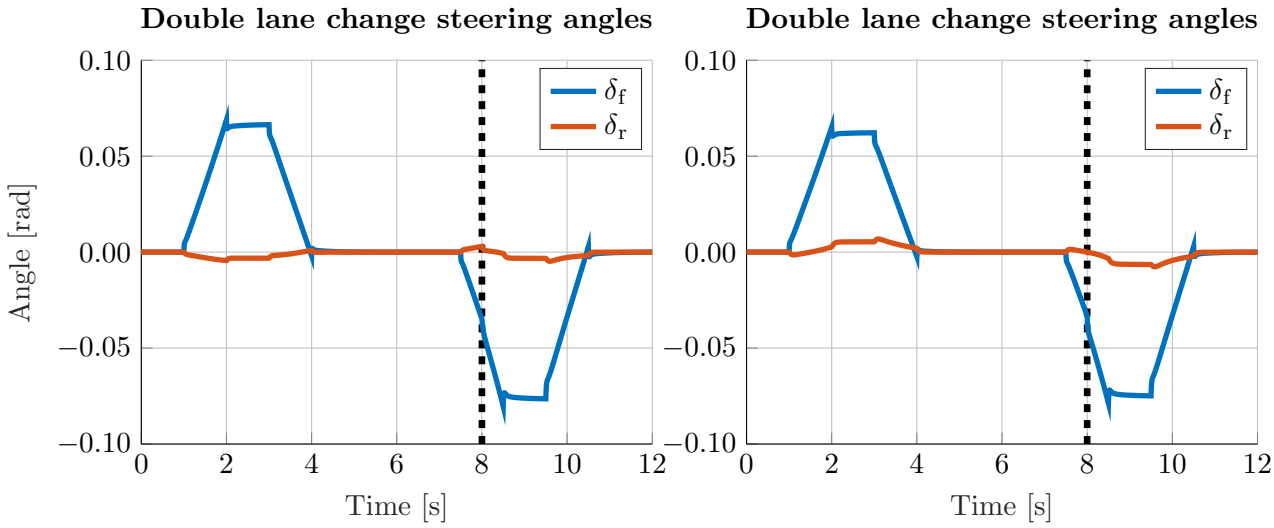

(a) The understeering behavior of the car (b) The oversteering behavior of the car

Figure 9.20: Difference α_i control steer angle inputs for double lane change maneuver for $v = 15\ \mathrm{m \cdot s^{-1}}$ where Pacejka coefficient D of rightside wheels is set to 0.4 in 8 s.

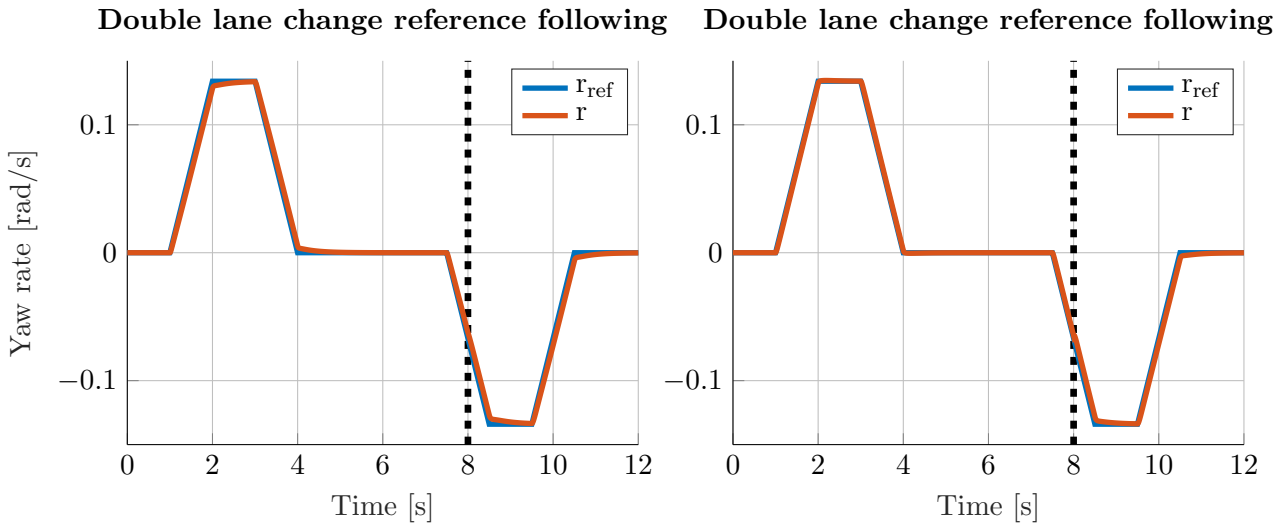

(a) The understeering behavior of the car (b) The oversteering behavior of the car

Figure 9.21: Difference α_i control reference following for double lane change maneuver for $v = 35\ \mathrm{m} \cdot \mathrm{s}^{-1}$ where Pacejka coefficient D of rightside wheels is set to 0.4 in 8 s.

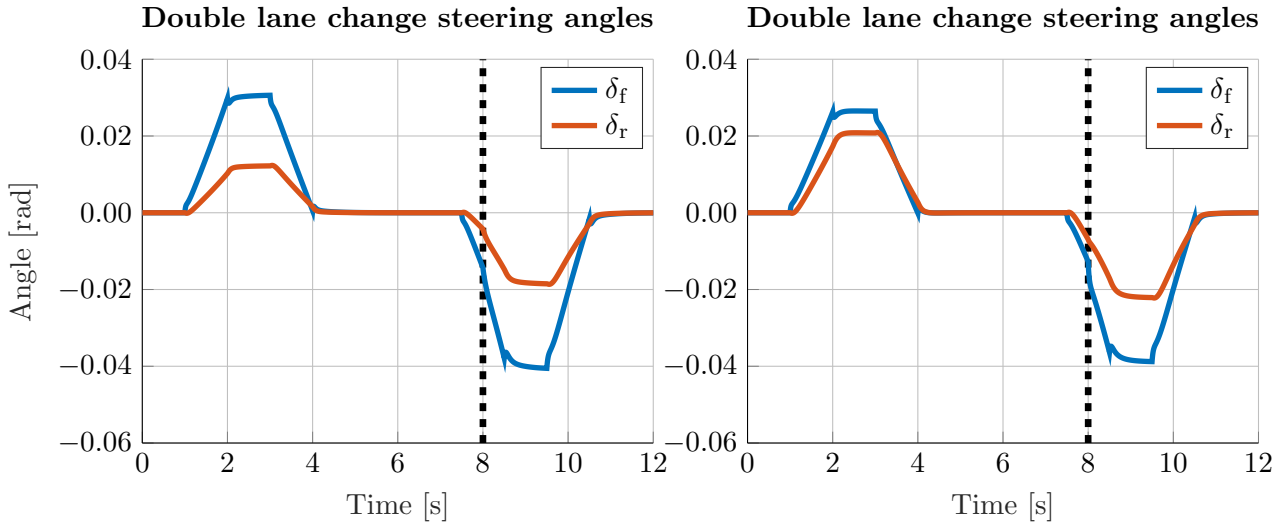

(a) The understeering behavior of the car (b) The oversteering behavior of the car

Figure 9.22: Difference α_i control steer angle inputs for double lane change maneuver for $v = 35\ \mathrm{m} \cdot \mathrm{s}^{-1}$ where Pacejka coefficient D of rightside wheels is set to 0.4 in 8 s.

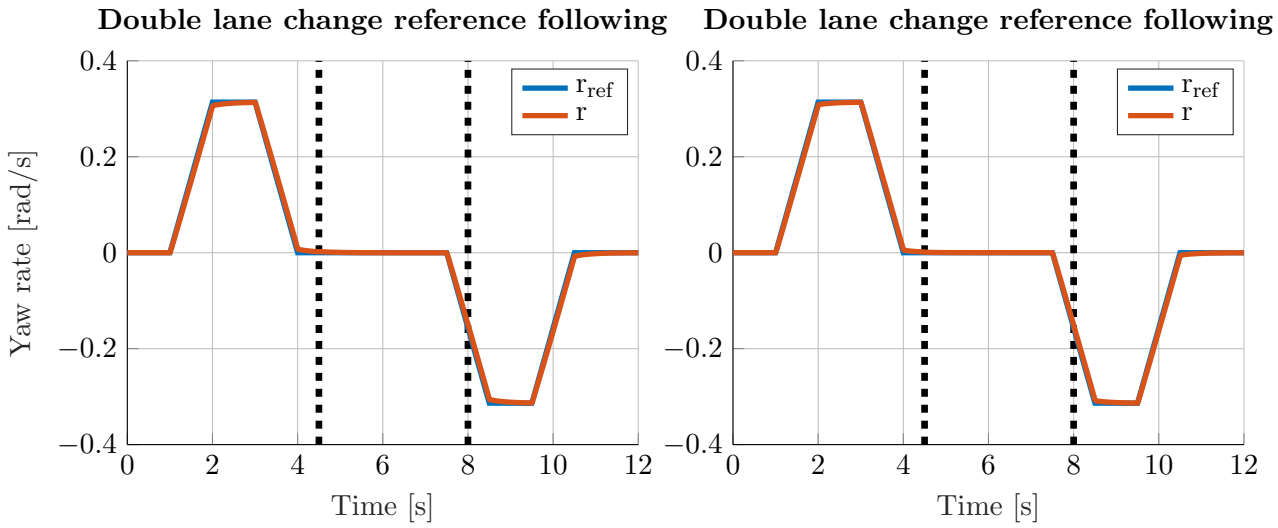

(a) The understeering behavior of the car (b) The oversteering behavior of the car

Figure 9.23: Difference of tyre slip angles control reference following for double lane change maneuver for $v = 15\ \mathrm{m} \cdot \mathrm{s}^{-1}$ for step-change of β as in [9.2].

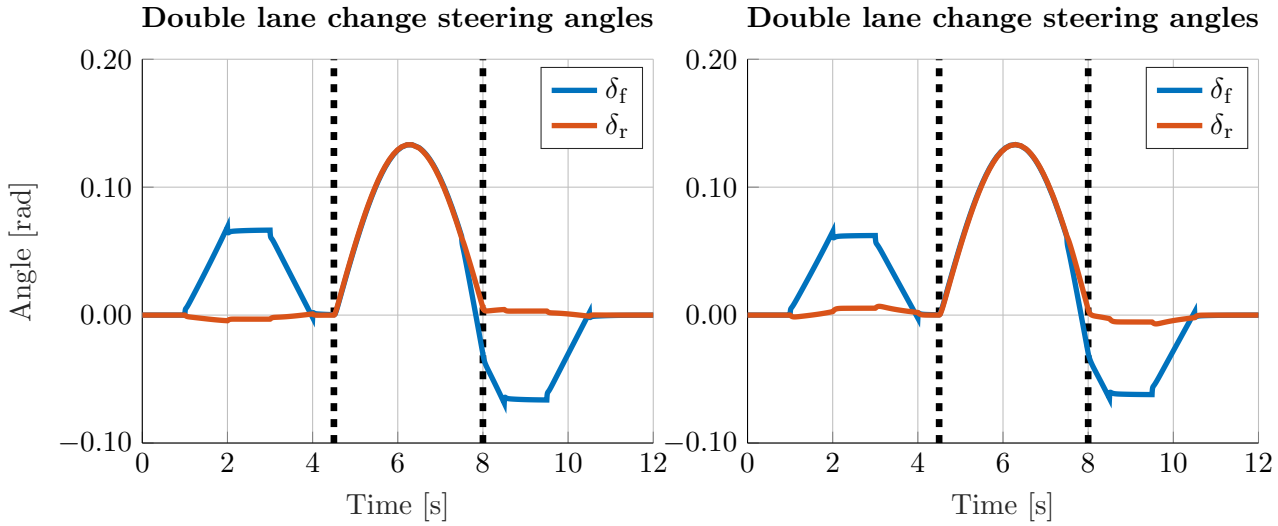

(a) The understeering behavior of the car (b) The oversteering behavior of the car

Figure 9.24: Difference of tyre slip angles control steer angle inputs for double lane change maneuver for $v = 15\ \mathrm{m} \cdot \mathrm{s}^{-1}$ for step-change of β as in [9.2].

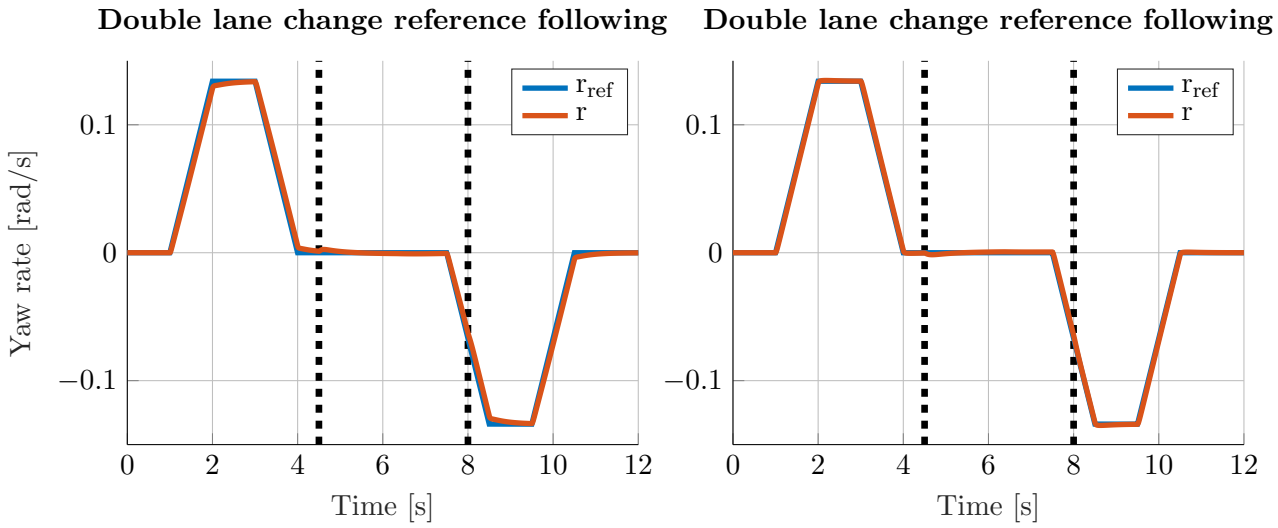

(a) The understeering behavior of the car (b) The oversteering behavior of the car

Figure 9.25: Difference of tyre slip angles control reference following for double lane change maneuver for $v = 35\ \mathrm{m} \cdot \mathrm{s}^{-1}$ for step-change of β as in [9.2].

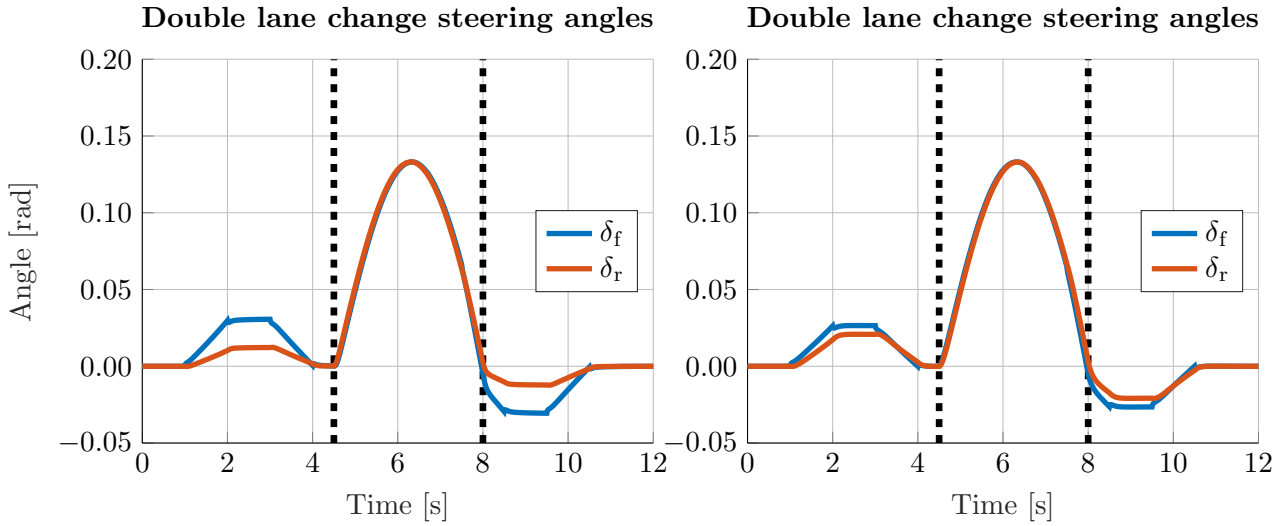

(a) The understeering behavior of the car (b) The oversteering behavior of the car

Figure 9.26: Difference of tyre slip angles control steer angle inputs for double lane change maneuver for $v = 35\ \mathrm{m} \cdot \mathrm{s}^{-1}$ for step-change of β as in [9.2].

From figures [9.19] and [9.24] can be evalueted that entry of only half of vehicles wheels on grass-rock surface has low or zero effect on regulation as well. Next, for the understeering behavior the sign of δ_r is changing according to velocity as in section [**Yaw-rate tracking test**] and mainly, there are no spikes due to step-change of side slip angle β. However, double lane change maneuver is better executed on the the oversteering behavior of the car. It is possible to choose bigger P constant for feedback of side slip angle β but testing has shown that steering angle δ_r then gets to saturation in more sharp manuevers and car can then lose stability on the road because it is unable to compensate given manuever more. Moreover, in provided simulator controller manage

to cut almost all too high yaw rate references for the understeering car that would lead to unstability, effectively lowering the posibility of human error.

9.6 Robust decoupling

The referenced steering wheel input in [9.1] is converted to front lateral acceleration a_{fref} by [**Input conversions**] using equation [9.7]. The controller is the same as in [**Robust decoupling**] with parametres from section [**Parameters**] and where $k_D = 1$.

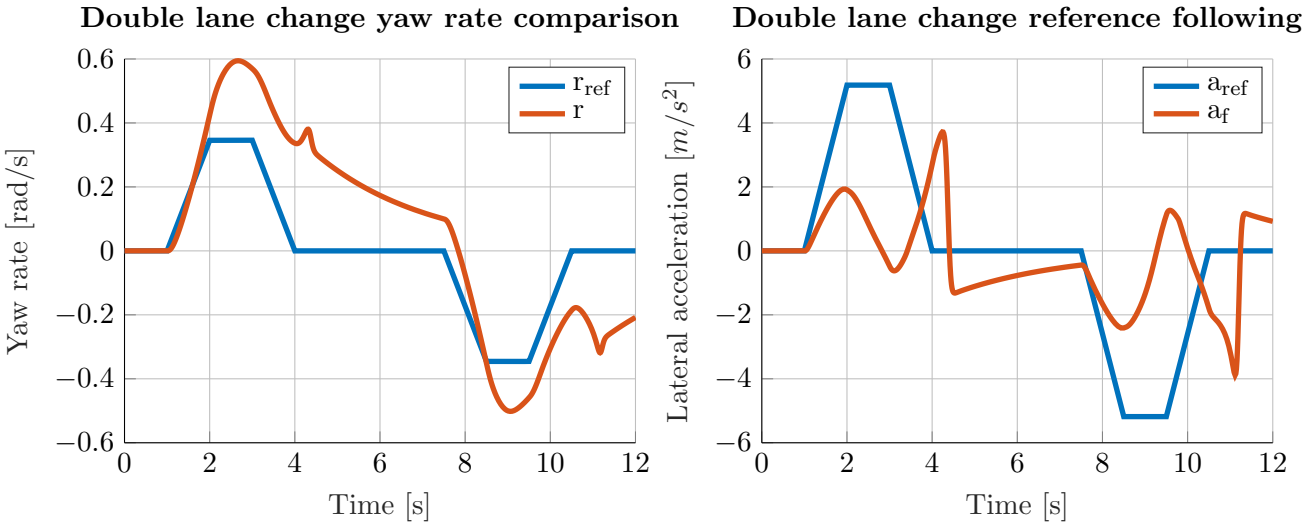

(a) Yaw rate comparison

(b) Front axle lateral acceleration following

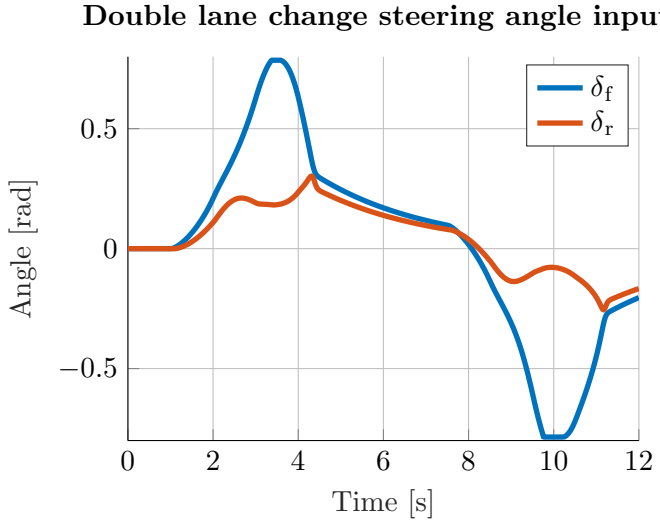

(c) Vehicle's steering angles

Figure 9.27: Double lane change reference following of the oversteering behavior of the car with parametres from section [**Parameters**] without any deviation for $v = 15\ \mathrm{m} \cdot \mathrm{s}^{-1}$.

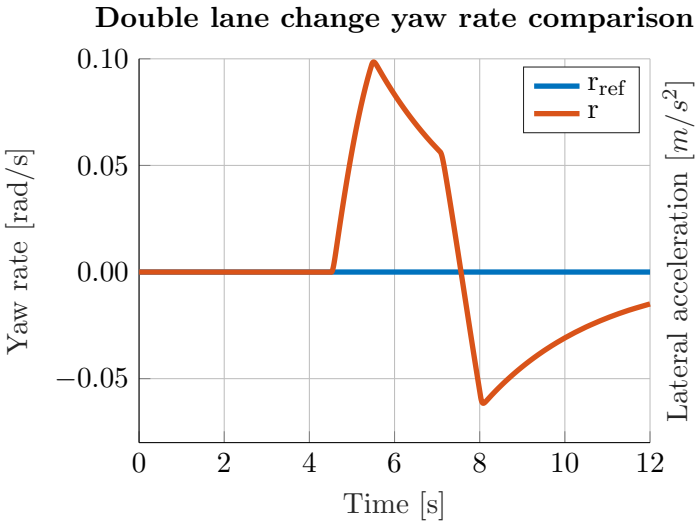

(a) Yaw rate comparison

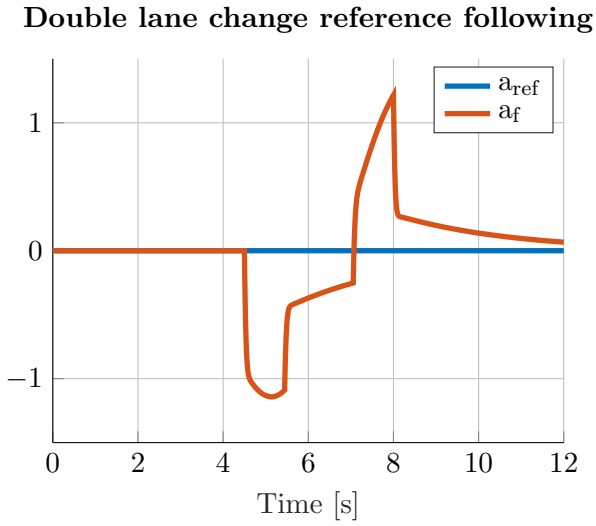

(b) Front axle lateral acceleration following

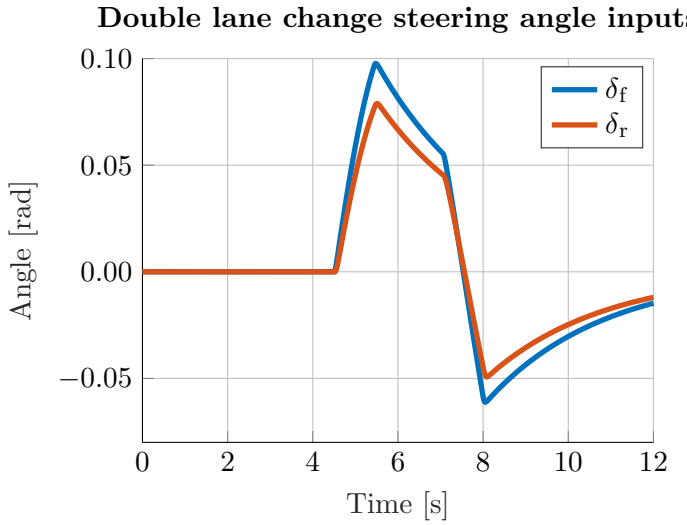

(c) Vehicle's steering angles

Figure 9.28: Stability on road with no reference following for step-change of β as in [9.2] for the oversteering behavior of the car with parametres from section [**Parameters**] for $v = 15\ \mathrm{m} \cdot \mathrm{s}^{-1}$.

As seen in [9.27], car is not following reference input and even when the reference becomes stable, system is still executing previous maneuver. Graph in [9.28] shows reaction of vehicle on a deviation caused by wind blowing to the side of the car where response of the controller is very slow and oscilatting. Even though, the k_S and k_D variables can be altered, the overall effect is still the same.

9.7 Rear wheel steering control

The referenced steering wheel input in [9.1] is converted to yaw rate r_{ref} by [**Input conversions**] using equation [9.6] and is followed by PI-controller with coefficients from [**Proposed control augmentation**] where the rear wheel control is from [4] and parametr l_3 is changed by I-controller.

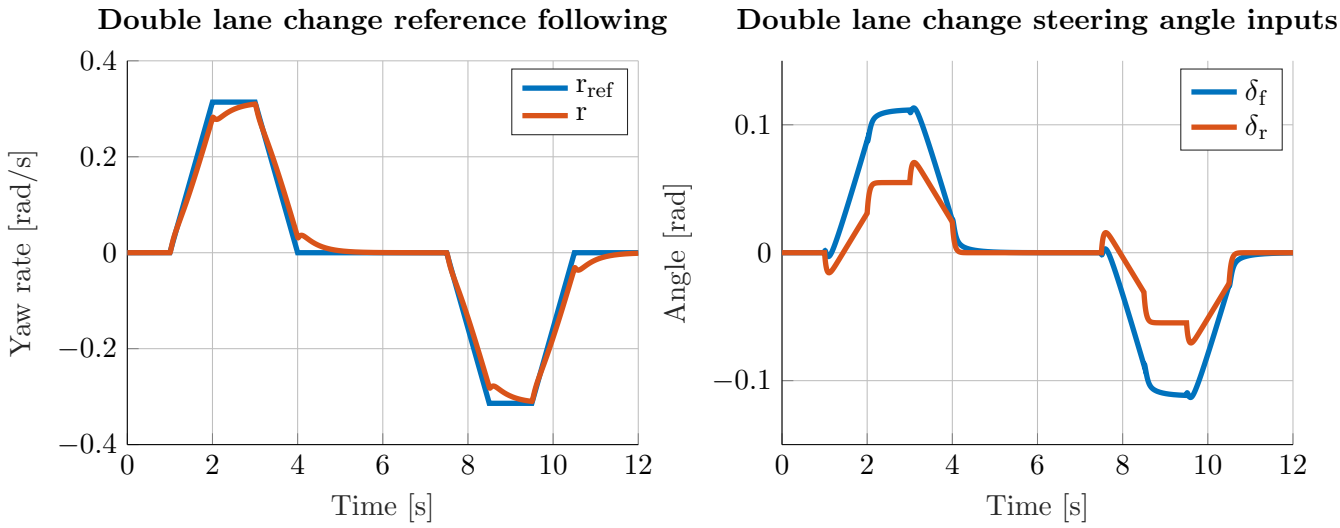

Figure 9.29: Double lane change reference following of the oversteering behavior of the car with parametres from section [**Parameters**] without any deviation for $v = 15$ m·s^{-1} where on the left side are yaw rates and on the right side steering angles of the vehicle.

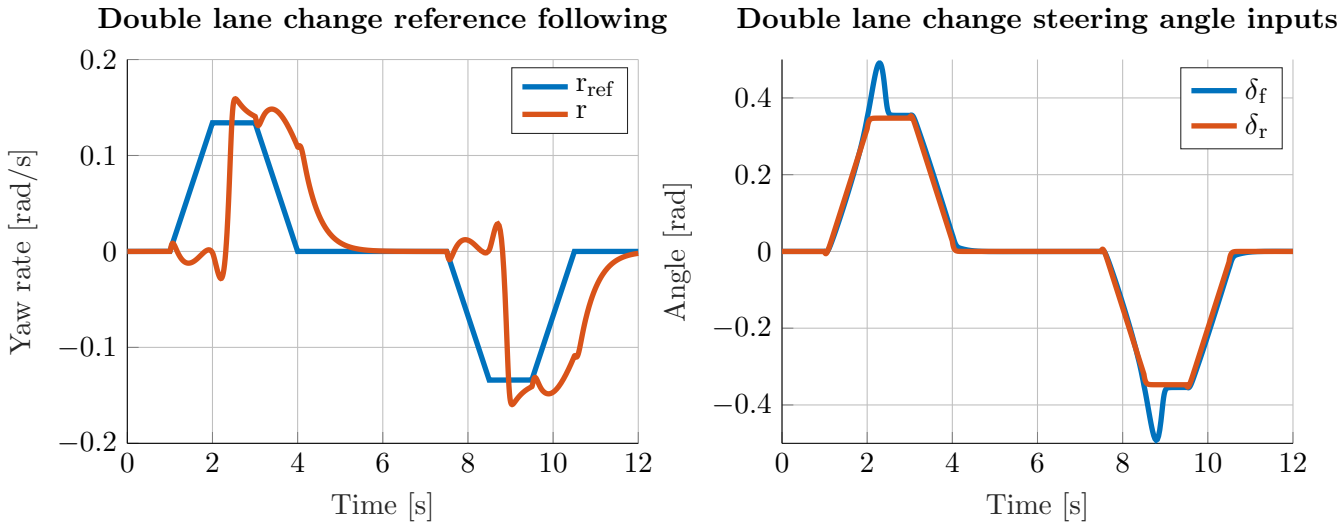

Figure 9.30: Double lane change reference following of the oversteering behavior of the car with parametres from [**Parameters**] without any deviation for $v = 35$ m·s^{-1} where on the left side are yaw rates and on the right side steering angles of the vehicle.

As seen in [9.29], vehicle is capable of following double lane change reference. However, from figure [9.30], when car is driving close to critical velocity. Which can be computed by formula [6.17] and equals to $v_{crit} = 46.9714$ m · s^{-1} for the the oversteering behavior of the car. Vehicle becomes unstable and because of no feedback to transfer function from company Nissan, car can become unpredictable and start spining which is not suitable for road car driving. Note that the same applies for system proposed by company Nissan, meaning no front steering control with only rear wheel feedforward as transfer function (6.15).

10. Results

All objectives of this work have been fulfilled:

- Non-linear single-track model has been adopted and disscussed in chapter [**Used modeling approaches**].
- Advantages and disdvantages of four-wheel steering car are listed in [**Introduction**].
- Review of state of the art is wrote down in chapter [**State of the art**].
- Imlementation of already published approaches are in chapters [**Robust decoupling**] and [**Rear wheel steer angle control system**].
- Control method improvements are listed in chapter [**Proposed solutions**] and in [**Rear wheel steer angle control system**] in section [6.4].
- Validation and testing is in chapter [**Simlutation ride tests**].

11. Conclusion

One of the main concerns of four-wheel steering systems is the connection of steering wheel to both car's axles. This work observed some of the already published solutions from industry and science, and proposed their alternations and new concepts that could be used.

The yaw stabilization is a very complex topic and can be achieved by many different solutions. The yaw rate tracking concept is highly efficient at low speeds, helping the car in cornering maneuvers. However, with higher velocity, poles of the system are shifted closer to the stability boundary. One of the approaches was to use control law mentioned in section [**First control law**] and even though, the integrator made zero deviation at low speeds, PI-controller was still required at a higher velocity, making car oscillate and eventually unstable (double integrator problem).

The feedback of side slip angle β is very useful because it keeps the car in a stable state and due to the capability of altering yaw rate r indirectly to β. Moreover, at a higher velocity, it is helping to system stability and reducing oscillations. During testing, feedback of referenced β_r was developed, which turned out to be very active in slip maneuvers, negating many chances of the car getting to spin, but it is main purpose is to stabilize the car and so it's usage in turn maneuvering is minimal.

Another possibility for δ_r control is to choose the same approach as in [1]. That is to calculate transfer function from input r_{ref} to δ_r with assumption of $\beta = 0$ and so $\dot{\beta} = 0$. It was not used here because during ride tests, the feedback of β has shown to be more effective. However, side slip angle β has to be estimated because it could not be directly measured. That is why, the transfer function could prove to be more trustworthy in real life car control if no direct measurement of β is provided.

The solution of Nissan company has no feedback control, and so it does not change vehicle dynamics. It is not suited for any oversteering vehicle, and even though, it is possible to improve this concept, for instance, using the proposed solution in [**Proposed control augmentation**], it is still not able to stabilize the car.

The standout concept is control based on the regulation of α_f with reference input that is calculated from the steering wheel. Because of the vehicle's tendency to actively try to minimize this angle, the control of the car is possible. Moreover, due to control of tyre slip angles, the ability of the car to slip is highly reduced and thus possible spinning as well.

The very promising solution is controller derived in chapter 4 in [**Difference of tyre slip angles**]. The poles are moving from the stable boundary with higher speeds, making it more stable. Moreover, the system can withstand very high environment deviations, shown in [**Difference of tyre slip angles test**]. Also, ride tests have shown that for understeering vehicle with CG in the front of the car, the controller is capable of cutting driver's input for infeasible cornering maneuvers, effectively lowering the possibility of human error.

Proposed controllers are tested on the single-track and twin-track models derived

in chapter [**Used modeling approaches**] and so further testing on real platforms will be needed. In the future work, the proposed concepts are very promising but their designs could be built upon and improved. The rear wheel steering is used mainly for stabilizing the oversteer tendency that used car has, but could be used to enhance performance in regular maneuvers as well.

12. Bibliography

[1] Ackermann, J. (1994). Robust decoupling, ideal steering dynamics and yaw stabilization of 4WS cars. *Automatica*, 30(11), 1761-1768.

[2] Schramm, D. and Hiller, M. and Bardini, R. (2014). Vehicle dynamics. *Modeling and Simulation.* Berlin, Heidelberg, 237-243, 255-298.

[3] Franklin, G. F. and Powell, J. D., Emami-Naeini, A., Powell, J. D. (1994). Feedback control of dynamic systems (Vol. 3). Reading, MA: Addison-Wesley.

[4] Mori, K. and Irie, N. (1990). U.S. Patent No. 4,947,326. Washington, DC: U.S. Patent and Trademark Office.

[5] *Documentation of Adams/Tire*, available on `http://mech.unibg.it/~lorenzi/VD&S/Matlab/Tire/tire_models_pac2002.pdf`

[6] Pacejka, H. (2005). *Tire and vehicle dynamics.* Elsevier.

[7] Haffner L. (2008) *Real-time tire models for lateral vehicle state estimation* (Doctoral dissertation). Retrived from Universitätsbibliothek der TU Wien.

[8] Ackermann, J. (2012). Robust control: Systems with uncertain physical parameters. Springer Science and Business Media.

[9] *The Advantages and Disadvantages of Four-Wheel Steering System*, available on `https://oards.com/four-wheel-steering-system-info/`

[10] Efremov, D. (2018), Unstable ground vehicles and artificial stability systems, Prague, 13-17.

[11] Tsurumiya, O., Izawa, M., Abe, M., and Nonaga, I. (1993). *U.S. Patent No. 5,189,616.* Washington, DC: U.S. Patent and Trademark Office.

[12] Sudale, S. (2016). *U.S. Patent No. 9,409,597.* Washington, DC: U.S. Patent and Trademark Office.

[13] Efremov, D., Haniš, T., and Hromčík, M. (2019). *Introduction of Driving Envelope and Full-Time-Full-Authority Control for Vehicle Stabilization Systems*, IEEE Xplorer.